geologicaacta

# Structure of an inverted basin from subsurface and field data: the Late Jurassic-Early Cretaceous Maestrat Basin (Iberian Chain)

**M. NEBOT and J. GUIMERÀ**

**Geomodels Research Institute, Departament de Geodinàmica i Geofísica, Facultat de Geologia, Universitat de Barcelona (UB)**
Martí i Franquès s/n, 08028 Barcelona, Spain.   Nebot   E-mail: marinanebotmiralles@gmail.com
Guimerà   E-mail: joan.guimera@ub.edu

┤ A B S T R A C T ├

The Maestrat Basin experienced two main rifting events: Late Permian-Late Triassic and Late Jurassic-Early Cretaceous, and was inverted during the Cenozoic Alpine orogeny. During the inversion, an E-W-trending, N-verging fold-and-thrust belt developed along its northern margin, detached in the Triassic evaporites, while southwards it also involved the Variscan basement. A structural study of the transition between these two areas is presented, using 2D seismic profiles, exploration wells and field data, to characterize its evolution during the Mesozoic extension and the Cenozoic contraction.

The S-dipping Maestrat basement thrust traverses the Maestrat Basin from E to W; it is the result of the Cenozoic inversion of the lower segment–within the acoustic basement–of the Mesozoic extensional fault system that generated the Salzedella sub-basin. The syn-rift Lower Cretaceous rocks filling the Salzedella sub-basin thicken progressively northwards, from 350m to 1100m. During the inversion, a wide uplifted area –40km wide in the N-S direction– developed in the hanging wall of the Maestrat basement thrust. This uplifted area is limited to the North by the E-W-trending Calders monocline, whose limb is about 13km wide in its central part, dips about 5ºN, and generates a vertical tectonic step of 800-1200m. We interpreted the Calders monocline as a fault-bend fold; therefore, a flat-ramp-flat geometry is assumed in depth for the Maestrat basement thrust. The northern synformal hinge of the Calders monocline coincides with the transition from thick-skinned to thin-skinned areas. The vast uplifted area and the low-dip of the monocline suggest a very low-dip for the basement ramp, rooted in the upper crust. The Calders monocline narrows and disappears laterally, in coincidence with the outcrop of the Maestrat basement thrust.

The evaporitic Middle Muschelkalk detachment conditioned the structural style. Salt structures are also related to it; they developed during the Late Triassic extension, as deduced from the Keuper seismic reflectors that onlap the folded Upper Muschelkalk and form growth strata above some basement normal faults.

## INTRODUCTION

The Iberian Chain, located in the eastern Iberian Peninsula (Fig. 1), is a fold-and-thrust belt that developed during the Cenozoic, due to the contractional inversion of the Mesozoic Iberian rift system (Álvaro *et al.*, 1979; Guimerà and Álvaro, 1990; Salas *et al.*, 2001). The Maestrat Basin, located in the eastern Iberian Chain, was one of the most subsident basins of the Mesozoic Iberian rift system during the Late Jurassic and Early Cretaceous. It contains up to 6.5km of Mesozoic sediments, among which up to 4km correspond to Upper Jurassic and Lower Cretaceous rocks (Fig. 2). It has been proposed that its formation was related to a system of listric extensional faults, some of them involving the Variscan basement. These faults bounded the basin, and also divided it into
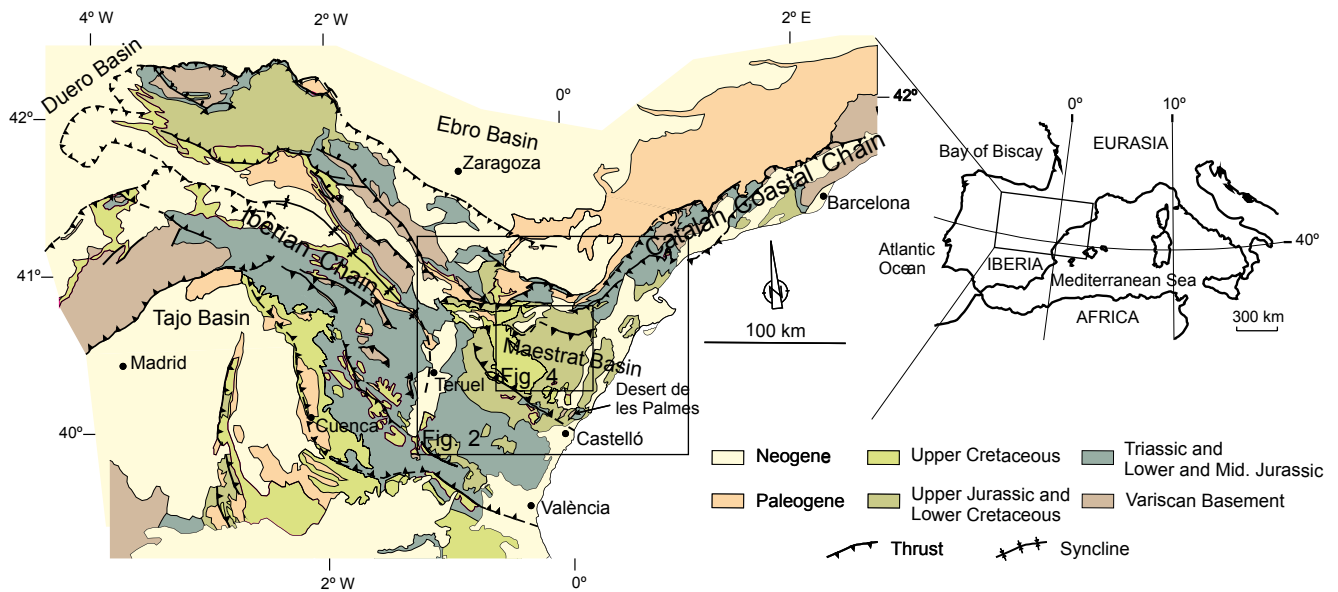
**FIGURE 1.** Structural map of the Iberian Chain and its location in the northeastern Iberian Peninsula (Modified from Guimerà, 2004, 2013).

sub-basins which contain different thicknesses of the Mesozoic sedimentary fill (Salas and Guimerà, 1996; Salas *et al.*, 2001).

An E-W-trending, N-verging, fold-and-thrust belt developed along the northern boundary of the Maestrat Basin as a result of the Cenozoic contraction (Guimerà, 1988). This belt involved the Mesozoic cover in the northern–foreland–areas, with detachment levels located within the Triassic evaporitic units. Southwards, the thrust system also involved the Variscan basement. The aim of this paper is to characterize the structure of the transition between the thin-skinned and the thick-skinned areas, which coincides at the surface with an approximately E-W-trending vertical tectonic step. The formation of this tectonic relief has been associated with the Turmell fault zone (Salas and Guimerà, 1996; González and Guimerà, 1997), a WNW-trending, S-dipping fault zone resulting from the inversion of the Mesozoic extensional fault system (González *et al.*, 1994; Guimerà and Salas, 1996). However, the Turmell fault zone does not match the structures that we recognize in the present study, so it is necessary to review this entire concept.

To this end, we studied the geometry and evolution of the Mesozoic and Cenozoic structures by integration of available subsurface data–2D seismic profiles and exploration wells–and new field data. Our results show that the wide uplifted area that developed during the Cenozoic inversion of the Maestrat Basin is bounded to the N by an E-W-trending monocline, the Calders monocline, which generates a tectonic relief. We interpret this monocline as a fault-bend fold developed in the hanging wall of a deep-

basement thrust, the Maestrat basement thrust, as a result of its flat-ramp-flat geometry. It becomes narrower laterally and is linked to the direct outcrop of the Maestrat basement thrust. In order to characterize the structure of the study region, we present five cross-sections and a reconstruction of specific geological surfaces as well as interpreted seismic profiles. The role of the thick Middle Muschelkalk evaporitic unit during extension and contraction is also considered.

## GEOLOGICAL SETTING

In the Iberian rift system, two major rifting cycles (Late Permian to Late Triassic, and Late Oxfordian to Late Albian) can be identified during the Mesozoic extension. Both were followed by episodes of lower rifting activity (Early and Middle Jurassic, and Late Albian to Maastrichtian) (Fig. 3, Salas *et al.*, 2001); although a more complex evolution has been observed in the study area, which is described below.

### Mesozoic rifting

The Late Permian to Late Triassic rifting was related to the westward propagation of the Tethys rift system and the southward propagation of the Arctic-North Atlantic rift system (Salas *et al.*, 2001). An intraplate rift system developed within the central and eastern Iberian plate during this period, the Iberian rift system (Álvaro *et al.*, 1979), bounded by high-angle normal faults. Sediments ranging from continental siliciclastics Upper Permian and Buntsandstein to marine carbonates (Muschelkalk) where

deposited (Salas *et al.*, 2001) as well as different evaporite units (Middle Muschelkalk and Keuper).

During the Early and Middle Jurassic post-rift period, a system of shallow carbonate platforms developed, covering the previously formed extensional structures. Angular unconformities between the Jurassic and the tilted Triassic rocks appear in several locations within the Maestrat Basin (Guimerà, 1988; Aurell *et al.*, 1992; Roca and Guimerà, 1992; San Román and Aurell, 1992; Roca *et al.*, 1994; Campos *et al.*, 1996).

The Late Oxfordian to Late Albian rifting is related to the opening of the North Atlantic Basin and the Bay of Biscay Basin, which separated Iberia from North America and Europe (Salas *et al.*, 2001; Salas *et al.*, 2010). During this rifting event, the carbonate platform system was broken and the Iberian Basin was divided into several separate basins. The Maestrat Basin (Fig. 2) is one of the most subsident basins that developed during this period (Salas and Guimerà, 1996; Salas *et al.*, 2001). A system of listric extensional faults developed, detached in the Triassic evaporitic units or within the Variscan basement, that divided the Maestrat Basin into different subsident blocs (Fig. 2). During this rifting event, a period of more moderate extensional activity occurred from the Late Valanginian to Late Hauterivian (Neocomian) in which thermal subsidence predominated (Salas and Casas, 1993; Salas *et al.*, 1995; Salas and Guimerà, 1996; Salas *et al.*, 2001; Salas *et al.*, 2010). Sediments of this age are lacking or partially eroded in some places of the Maestrat Basin.

During the Late Albian to Maastrichtian post-rift period, Iberia became separated from Europe and basin evolution was controlled by thermal subsidence and a rise in sea level (Salas *et al.*, 2001). The fluvial sediments of the Utrillas Formation (Late Albian to Cenomanian) were deposited unconformably over the previously formed extensional basins. During the Cenomanian to Turonian marine transgression, carbonate platforms developed that connected the Atlantic and the Tethys oceans. By the end of the Cretaceous, the whole area of the Iberian rift system was emerged and lacustrine sediments were deposited (Salas *et al.*, 2001) that may contain a few marine intercalations (Gautier and Barnolas, 1979).

### *Maestrat Basin*

The Maestrat Basin (Fig. 2) is bounded by two systems of listric extensional faults. The northern system is formed by WNW-trending, S-dipping listric normal faults (including the Turmell fault zone), while the southwestern system is oriented NW-SE and is mostly NE-dipping. The double rollover geometry of the hanging walls of these listric faults generated the Salzedella sub-basin to the N
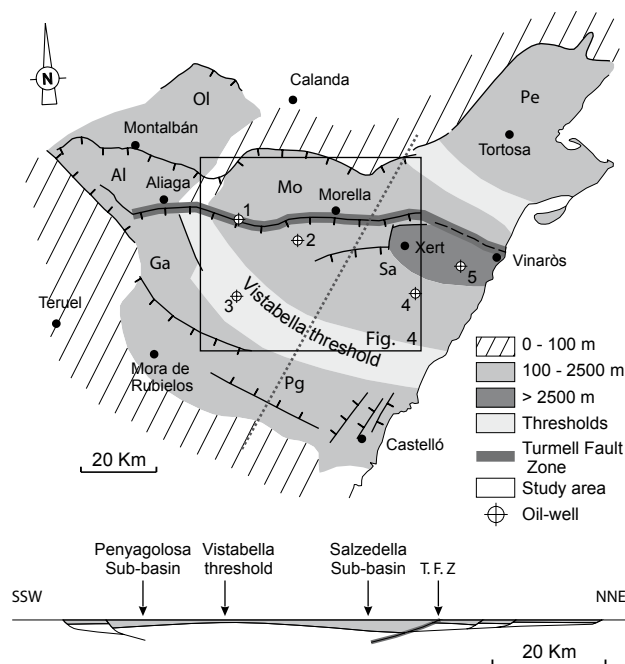


**FIGURE 2.** Simplified map of the Maestrat Basin during the Late Jurassic-Early Cretaceous rifting event. The basin was divided into several sub-basins: Ol= Oliete sub-basin, Al= Aliaga sub-basin, Mo= Morella sub-basin, Pe= Perelló sub-basin, Ga= Galve sub-basin, Sa= Salzedella sub-basin and Pg= Penyagolosa sub-basin. Wells: 1= Mirambell-1, 2= Bovalar-1 and Bovalar-2, 3= Maestrazgo-2, 4= Salzedella-1, 5= Maestrazgo-1. Modified from Salas and Guimerà (1996) and Salas *et al.* (2005).

and the Penyagolosa sub-basin to the S, separated by the Vistabella threshold (Fig. 2) (Salas and Guimerà, 1996; Salas *et al.*, 2005). The E-W-trending Turmell fault zone is interpreted to be the main normal fault in the northern side of the Maestrat Basin (Fig. 2). It separates the more subsident inner part (Salzedella and Galve sub-basins) in its hanging wall (S) from its outer part (Morella and Aliaga sub-basins) in its footwall (N) (Salas and Guimerà, 1996).

The Maestrat Basin succession (Fig. 3) is mainly composed of shallow marine to lacustrine carbonates with intercalations of continental siliciclastic sediments (Early Aptian Morella Fm. and Early Albian to Cenomanian Escucha and Utrillas fms.) and a few intercalations of pelagic sediments. Valanginian-Hauterivian sediments are not represented in the western Salzedella sub-basin (Fig. 3).

### Cenozoic Alpine contraction

The contractional deformation, related to the Alpine orogeny during which Iberia and Europe were again connected, occurred in the Maestrat Basin during the Late Eocene to Early Miocene (González, 1989). The inversion of the Maestrat Basin gave rise to the linking zone between the Iberian Chain and the Catalan Coastal Chain, with NW-SE and NE-SW structural trends, respectively
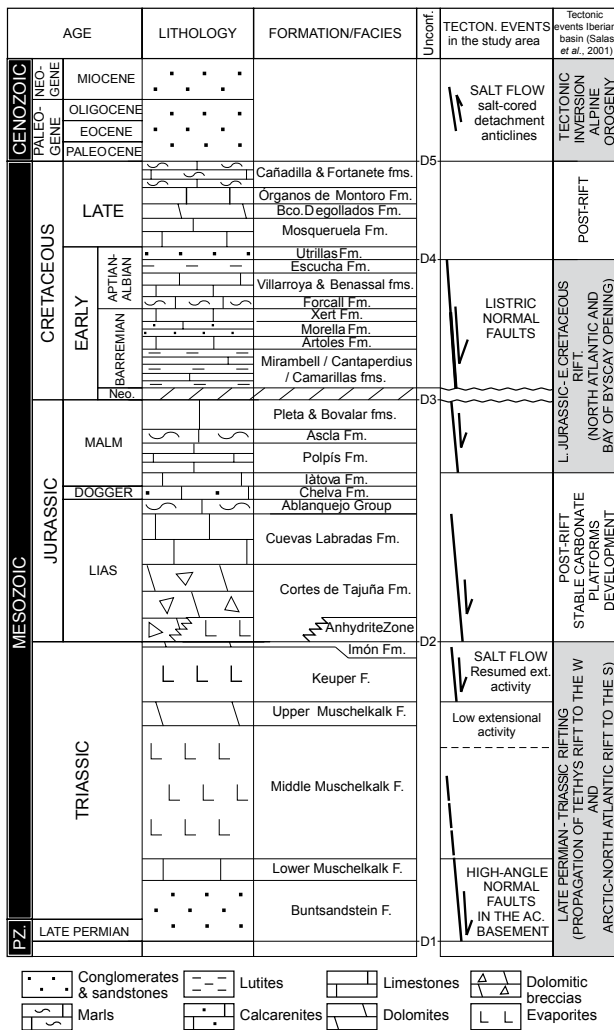
**FIGURE 3.** Tectonostratigraphic chart of the Maestrat Basin in the surroundings of the Mirambell-1 well (W Salzedella sub-basin). The different formations, their age and lithologies are shown. Abbreviations: Ac= Acoustic; Fm= Formation; F= facies; Neo= Neocomian (Berriasian, Valanginian and Hauterivian). The tectonic events described in the study area and those described by Salas et al. (2001) for the whole Iberian Basin, are indicated in the two right columns. Based on Canérot et al. (1982), Salas (1987) and Bover-Arnal et al. (2016) for the Barremian-Aptian boundary.

(Guimerà, 1988; Salas et al., 2001). The Linking Zone is characterized by approximately E-W-trending, N-verging thrusts and folds, with a few areas where structures display virgation, and NE-SW and NW-SE structures appear (Guimerà, 1988). A detachment level is located within the Triassic evaporitic units in the North, and towards the S, the thrust system also involved the Variscan basement in the Turmell fault zone, (González and Guimerà, 1997). A roughly N-directed displacement direction was deduced for the linking zone thrust sheets (Guimerà and Álvaro, 1990). The Cenozoic inversion of the Turmell fault zone raised its hanging wall, generating a wide elevated area and a vertical tectonic step between the uplifted hanging wall and the footwall (González et al., 1994; González and Guimerà, 1997). The internal deformation in the cover of this elevated area decreases towards the S (Guimerà, 1988), and resulted in a zone characterized by large folds (up to 25-30km along the trend) of long wavelengths (about 5km).

The uplifted area extends beyond the study area. It is nearly 40km wide in the NNE-SSW orientation, and more than 90km long in the E-W orientation, from the easternmost segment of the Turmell fault (Fig. 4) to the southern boundary of the Cenozoic Aliaga Basin (González and Guimerà, 1993; Guimerà and Salas, 1996). In it, a topographically elevated area (1300 to 2000m a.s.l.) containing Upper Cretaceous and Cenozoic rocks –the youngest pre-contractional rocks– is still preserved (Guimerà et al., 2010).

The study area (Figs. 1; 2; 4) covers the western part of the Salzedella sub-basin, the Turmell fault zone (as defined by Salas and Guimerà, 1996) and the southern part of the fold-and-thrust belt North of the Turmell fault zone.

## DATASET AND METHODOLOGY

### Data

The seismic dataset (Fig. 5) comprises 29 2D seismic reflection profiles obtained in 1973 by Auxini, in 1979 by Campsa and in 1987-88 by Shell in the Maestrat Basin. Four oil exploration wells were used to constrain the seismic interpretation and the construction of the cross-sections: Mirambell-1, drilled by Auxini in 1974; Maestrazgo-2, by Campsa in 1981; and Bovalar-1 and Bovalar-2, drilled in 1963 by Coparex. Some of the subsurface data were collected from the Instituto Geológico y Minero de España (SIGECO) and from the Archivo Técnico de Hidrocarburos web databases. The other seismic profiles were scanned from printed copies.

More than 1000 strike-and-dip data were collected in the field; while another 750 strike-and-dip data were obtained after drawing the geological contacts on the ortho-images and the 3D topographic contour lines in a georeferenced environment (Microstation), using in-house macros developed by Fernández (2004). The 3D visualization, using Global Mapper, of the ortho-images draped on the DTM and their comparison with data collected in the field allowed us to monitor the quality of the in-room dip data.

### Methods

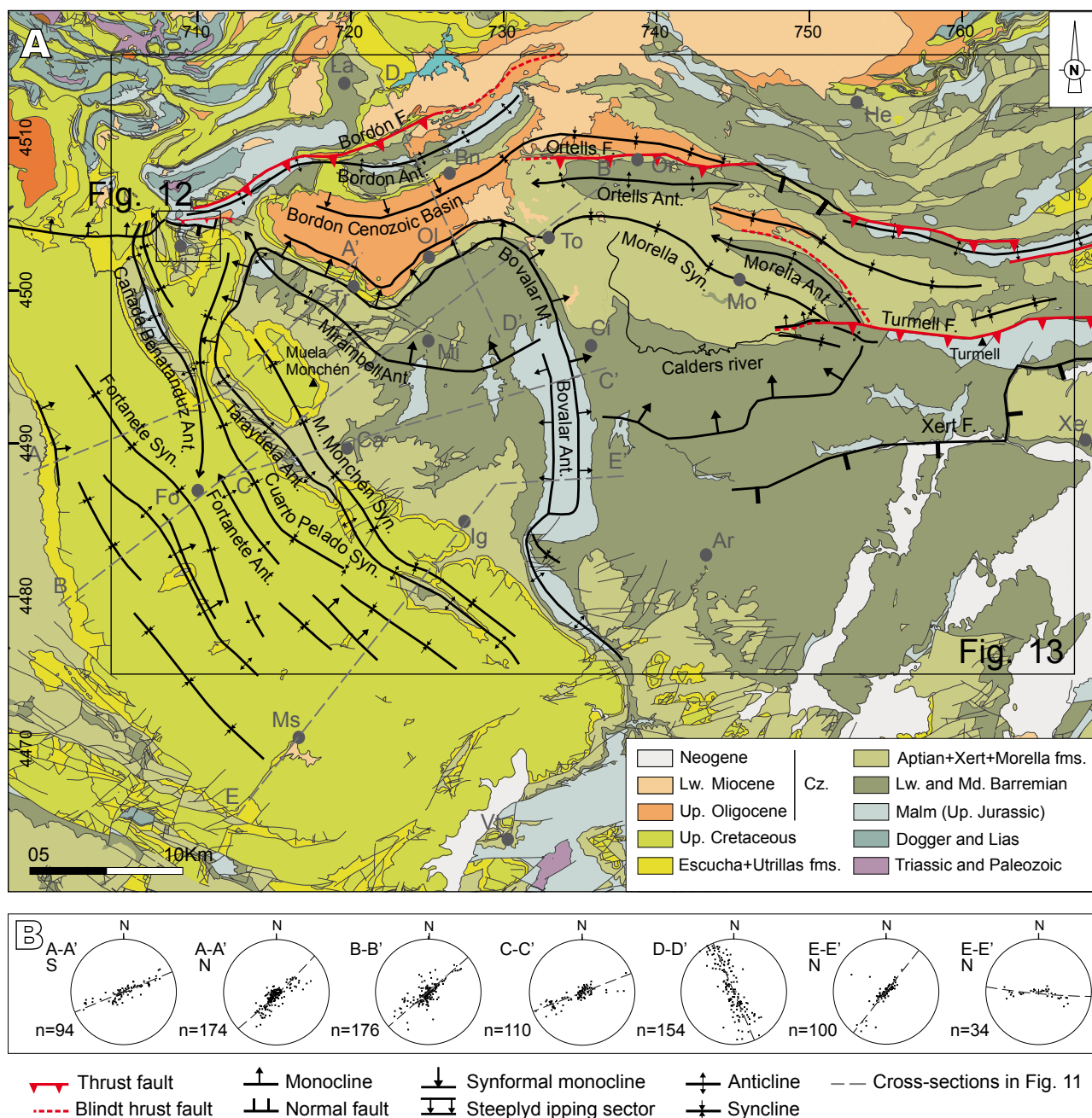Seismic profile images were converted to seg-y files using the IMAGE2SEGY Matlab application (Farran,

**FIGURE 4.** A) Simplified geologic map of the study area. Modified from the 1:50.000 IGME Magna geologic maps: Almera *et al.* (1982); Canérot and Leyva (1972); Canérot and Pignatelli-García (1972, 1977); Canérot *et al.* (1977); Esnaola and Canérot (1972); Gautier (1978, 1979); Martín *et al.* (1972); Navarro-Vázquez *et al.* (1972); Trell *et al.* (1979). Fold and fault trends are based on field observations and ortho-images interpretation. See location in Figure 1 and 2. Villages: Ar= Ares del Maestrat, Bn= Bordón, Ca= Cantavieja, Ci= Cinctorres, Fo= Fortanete, He= Herbés, Ig= La Iglesuela del Cid, La= Ladruñán, Mi= Mirambell, Mo= Morella, Ms= Mosqueruela, Ol= Olocau del Rei, Or= Ortells, To= La Todolella, Tr= Tronchón, Vl= Villarluengo, Vt= Vistabella del Maestrat, Xe= Xert. Abbreviations: Ant.= anticline, Syn.= syncline, M.= monocline, F.= fault. The location of cross-sections in Figure 11 is shown. UTM projection (zone 30, coordinates in km), ED50 datum. B) Lower hemisphere spheric equal-area projection of S0, showing the bedding orientation at different sectors of the study area, corresponding to the chosen cross-section traces. n= number of data.

2008) and interpreted using the Kingdom Suite software in a georeferenced environment. The seismic interpretation was constrained with the Mirambell-1 well tops, previously converted to two way time (TWT) with the velocities obtained from its sonic-log (Replacement velocity: 3250m/s, Cretaceous: 4985m/s, Jurassic and Imón Fm.: 5043m/s, Keuper and Upper Muschelkalk: 3491m/s, Middle Muschelkalk: 5441m/s). Seismic interpretation was converted to depth in meters using the same velocities obtained from the Mirambell-1 sonic-log.
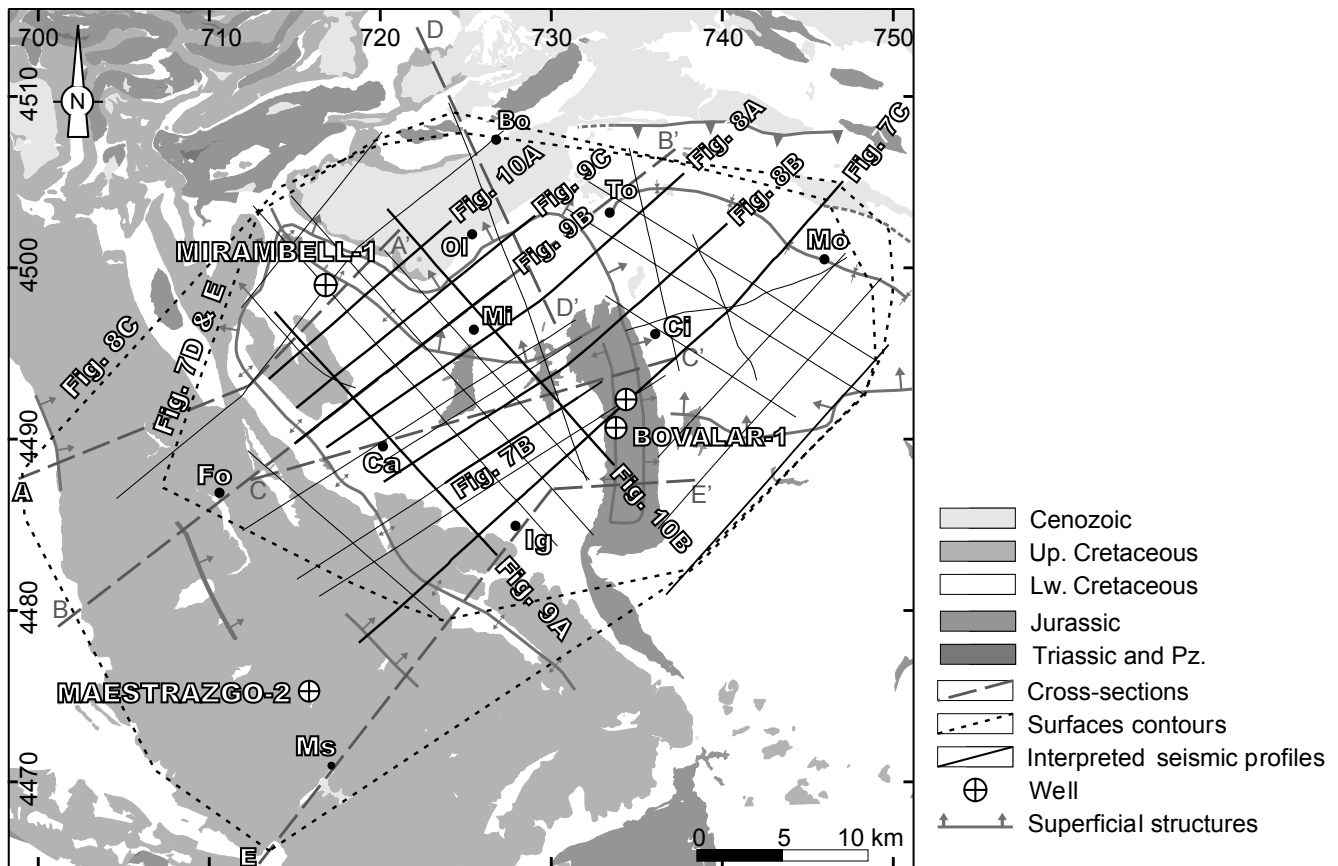
**FIGURE 5.** Location of the seismic profiles and exploration-wells used for the construction of cross-sections and geological surfaces, whose location is also shown. A simplified geological map and some main structures are shown for reference. UTM projection (zone 30, coordinates in km), ED50 datum.

Five cross-sections were constructed, normal to the different orientations of faults and axial fold planes observed in the study area (Fig. 4), in order to better characterize the geometry of the differently oriented structures.

Although the sections do not contain the roughly N-directed deduced displacement of the linking zone (Guimerà and Álvaro, 1990), and so are not restorable, they were unfolded using the flexural slip unfolding algorithm and the Upper Cretaceous base as a datum, in order to display the geometry of the syn-rift units. Cross-sections are based on field data, wells, and seismic interpretation converted to depth. Cross-section construction–using the Kink method–as well as unfolding were done both with Move and manually with Microstation software. Area conservation was assumed for the evaporitic units.

Two geological surfaces, the depth to the base of the Jurassic and the depth to the top of the acoustic basement, and the vertical thickness of the Middle Muschelkalk evaporitic unit were constructed with Gocad, based on seismic interpretation converted to depth, cross-sections and wells. The contours were later manually modified to better fit the structural trends and geometries.

## INTERPRETATION OF THE SEISMIC PROFILES

Six stratigraphic units were differentiated in the seismic profiles (Fig. 6), attributed to the Cretaceous (K), Jurassic (J), Keuper (TrK), Upper Muschelkalk (TrM3), Middle Muschelkalk (TrM2), and the acoustic basement (Bs) (which includes the Lower Muschelkalk, Buntsandstein and the Variscan basement). Their correspondence with the seismic facies was established from the Mirambell-1 well tops in TWT (s).

The top of the acoustic basement–top of the Lower Muschelkalk carbonate unit and base of the Middle Muschelkalk salt unit–is characterized by a couple of seismic reflectors of near-constant thickness (Fig. 6). The Upper Muschelkalk is characterized by three parallel seismic reflectors that have an almost constant thickness throughout the seismic profiles. This unit is located between two transparent seismic facies that correspond to the Triassic evaporitic units: the Middle Muschelkalk unit below and the Keuper unit above. The latter unit has a variable seismic facies, showing parallel reflectors in some places. A couple of seismic reflectors of constant thickness are also

present at the base of the Jurassic unit, which are mainly parallel to the Upper Triassic Keuper reflectors, although, as previously explained, an angular unconformity has been recognized at the base of the Jurassic in other marginal places of the basin. The Imón Fm. (Fig. 3) is located below the Jurassic but it is too thin (about 30m) to be recognized in the seismic profiles. Above this couple of seismic reflectors, the Lower Jurassic is characterized by transparent seismic facies, with some discontinuous parallel seismic reflectors. That corresponds to the dolomitic breccias of the Cortes de Tajuña Fm. (Hettangian) (Fig. 3). In the Mirambell-1 well, about 100m of anhydrite intercalations were identified at the base of the Jurassic. That may be related to the "Anhydrite zone" or Lécera Fm. (Rhaetian-Hettangian age; Castillo Herrador, 1974; Gómez and Goy, 1998) equivalent in age to breccias of the Cortes de Tajuña Fm. (Fig. 3). This "Anhydrite zone" does not crop out in the study area. At the surface, the Cortes de Tajuña breccias overlie the Imón Fm., without the presence of evaporites. The Upper Lias and Dogger units have almost transparent facies with some quite continuous reflectors, and the Malm unit is characterized by continuous parallel seismic reflectors. The Cretaceous is characterized by continuous parallel seismic reflectors, but more separated than those of the Malm, indicating higher wavelength.

## MESOZOIC EXTENSIONAL STRUCTURE OF THE ACOUSTIC BASEMENT AND RELATIONSHIP WITH THE TRIASSIC DETACHMENT LEVEL

Different evaporitic units have been identified in the study area: the Middle Muschelkalk and Keuper units, and, locally, the Lower Jurassic Anhydrite zone or Lécera Fm. (Fig. 3).

The Middle Muschelkalk is composed of halite and anhydrite with lutite intercalations (Lanaja, 1987; Martínez-Abad, 1991). It constitutes the main detachment level, differentiating the structural deformation styles between the acoustic basement and the supra-salt Mesozoic cover. The interpretation of the seismic profiles allowed us to characterize the structural style of deformation in the basement, which is not always reflected in superficial structures, and also revealed some salt-related structures developed in the Middle Muschelkalk.

### Structural style of the acoustic basement

Although the top of the acoustic basement–and base of the Middle Muschelkalk evaporitic unit–is not always easily recognized due to the quality of the seismic data, the network of seismic profiles allowed us to reconstruct this surface. We devised contour maps of the depth to the top of the acoustic basement (Fig. 7D) and of the present
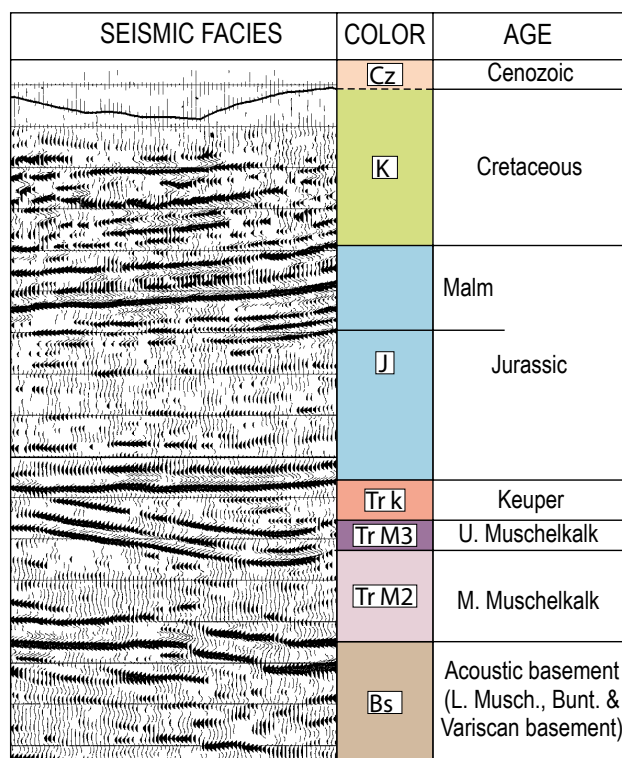


**FIGURE 6.** Seismic facies and horizons interpreted in the seismic profiles, and their correlation to the stratigraphy of the studied area. The Imón Fm. (Upper Triassic) is included in the impedance contrast at the base of the Jurassic, and is too thin (~30m) to be differentiated. The seismic-line shown is a segment of the northern part of the seismic profile CT88-15 (Fig. 8A).

vertical thickness of the Middle Muschelkalk evaporitic unit (Fig. 7E). We took into account the fact that the surface representing the top of the acoustic basement was not restored to its Late Triassic stage. However, some non-inverted Triassic structures could be identified in the seismic profiles and permitted us to study the Triassic extensional event.

The acoustic basement is affected by a set of high-angle normal faults, developed during the Late Permian to Late Triassic rifting event, which are mainly oriented NW-SE to WNW-ESE, and some N-S (Fig. 7D, E). These faults have lengths between 2 and 7km, and dip-slips up to 500m, defining a system of horsts, grabens and half-grabens. Two NW-SE-trending basement highs were recognized. The western one (Monchén basement high, located under the Muela de Monchén) is a horst bounded by NW-SE normal faults (Fig. 7A, D). The eastern one (Iglesuela basement high, located North of Iglesuela del Cid village) is bounded to the S by a S-dipping normal fault; whereas on the northern side, the basement progressively deepens to the North and northeast (Fig. 7B, D). This could be a consequence of a SW-dipping
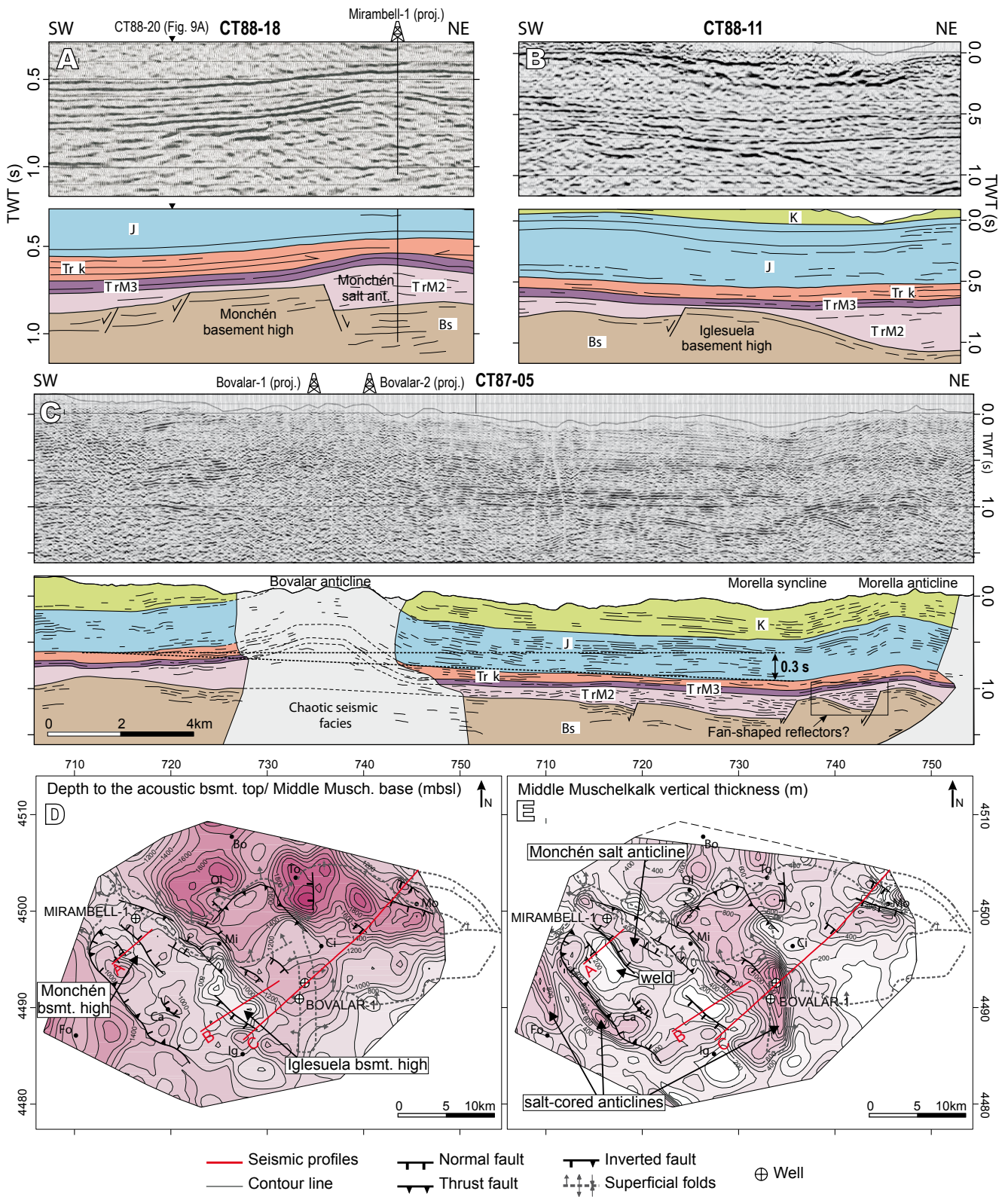
**FIGURE 7.** A, B) Details of seismic profiles CT88-18 (Fig. 10A) and CT88-11 and their interpretation, showing transversal sections of the Monchén and Iglesuela basement highs, respectively. C) Seismic profile CT87-05 and its interpretation. See Figure 6 for legend. D) Contour map of the depth to the top of the acoustic basement, *i.e.* base of the Middle Muschelkalk evaporitic unit (in m below the sea level). E) Contour map of the Middle Muschelkalk vertical thickness (in m). See Figure 5 for location. The location of A, B and C is shown in D and E. UTM projection (zone 30, coordinates in km), ED50 datum.

normal fault located N of the basement high, like those shown in Figure 8B.

**Middle Muschelkalk thickness variations**

North and east of the Iglesuela basement high, a NW-SE strip with a thick Middle Muschelkalk salt unit is identified, coinciding with the deeper basement. In the eastern part of this strip, the N-S-trending Bovalar detachment anticline developed, accumulating in its core more than 1200m of Middle Muschelkalk salt, as found in the Bovalar-2 well (Lanaja, 1987), located near the anticline hinge (Fig. 7D, E).

North of the Monchén basement high, another NW-SE strip of thickened Middle Muschelkalk evaporites is present: the Monchén salt anticline. It developed in the footwall of the normal fault that bounds the Monchén basement high to the N (Figs. 7; 9). This salt accumulation was pierced by the Mirambell-1 well, cutting through more than 625m of Middle Muschelkalk salt. 2km south of it, over the Monchén basement high, less than 100m of Middle Muschelkalk were identified in the seismic lines (Fig. 7A). It even disappears locally, as a salt weld is also observed above this basement high (Figs. 7E; 9A).

In the NE of the area studied, beneath the Morella syncline and anticline, some half-grabens can be observed (Fig. 7C), generated by S-dipping and probably WNW-ESE trending high-angle normal faults that displace the acoustic basement (Fig. 7D, E). The Middle Muschelkalk unit displays salt wedges thickening towards these faults and some fan-shaped reflectors can be identified against one of these faults (Fig. 7C highlighted in a box).

East of the area studied, near the Mediterranean coast, the exploration wells (Fig. 2) reveal that no Muschelkalk sediments are present. In the Salzadella-1 well, the Buntsandstein facies (70-150m) are overlaid by only 30m of Keuper clay and sandstone and in the Maestrazgo-1 well by about 250m of Keuper, composed mostly of halite and clay (Martínez-Abad, 1991). Southwards, in the Desert de les Palmes area, N of Castelló (Fig. 1), the Upper Muschelkalk overlies the Buntsandstein (Escudero-Mozo et al., 2015), and consists of about 100m of carbonate rocks, with no evaporites (López-Gómez et al., 2005).

**Interpretation of the basin evolution during the Late Permian-Triassic rifting event**

***Timing of the Triassic extensional faults***

Although the different units that form the acoustic basement cannot be distinguished in the seismic profiles,

in accordance with Álvaro et al. (1979) and Salas et al. (1997) the Triassic extensional faults involve the Late Permian to Middle Muschelkalk evaporitic unit, at least its lower part (Bartrina and Hernández, 1990), which fills the relief generated by the system of horsts, grabens and half-grabens, while its upper part overlies all these structures.

Considering the flow capacity of the Middle Muschelkalk evaporitic unit, it cannot be completely ascertained whether normal faults were active or not during its deposition. However, in view of the salt distribution, at least the lower part of the Middle Muschelkalk was deposited during extension, because the maximum thicknesses of this unit coincide with the depressed blocks of the acoustic basement, and the minimum thicknesses with the acoustic basement highs. This structure is overlain by the subhoritzontal supra-salt cover, indicating that no changes occurred in the salt thickness after deposition (Fig. 7B). The fan-shaped reflectors towards one of the acoustic basement faults previously reported (Fig. 7C highlighted in a box) should also be taken into account; they indicate that no salt motion occurred there, with the original salt thickness being preserved. What seems clear is that the Upper Muschelkalk carbonate platform was deposited in a period of little extensional activity, as an almost constant thickness of this unit is observed in the seismic profiles. It is only affected by some faults that are not associated with thickness variations in this unit (Fig. 9A, C).

The extensional activity of some normal faults resumed during the Keuper deposition, as can be deduced from the extensional drape fold that affects the Upper Muschelkalk carbonate platform above the basement faults (Fig. 9C), which does not involve the younger Mesozoic cover. The Keuper seismic reflectors onlap these Upper Muschelkalk folds (Fig. 9B, C). In profile CT88-17 (Fig. 9C), some growth strata can be identified in the Keuper, over the downthrown block of the basement fault, indicating extensional activity of the basement faults while the Keuper facies was being deposited.

***Salt-related structures that developed during Triassic extension***

As mentioned above, Middle Muschelkalk thickness variations are mainly syn-depositional; although, we cannot definitively ascertain whether the entire evaporitic unit was deposited during extension. However, there is also evidence of salt flow that would have enhanced these thickness variations in some areas, as some salt-related structures can be observed in the seismic profiles.

As opposed to what happens in other Iberian locations, where salt tectonics is related to the Keuper
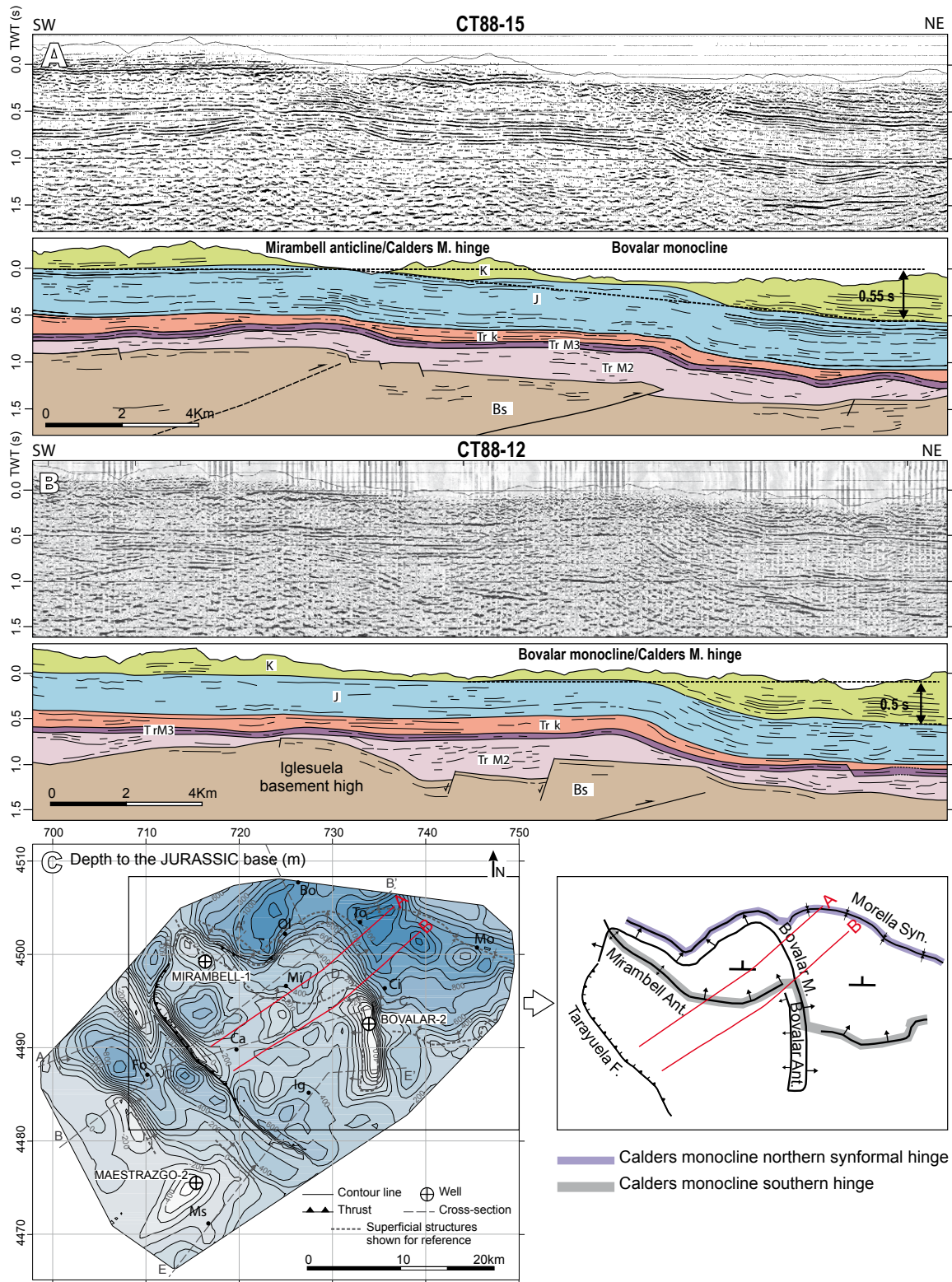
**FIGURE 8.** A) Seismic profile CT88-15 and its interpretation. The tilted limb of the Calders monocline and its southern hinge –which is the transition from the tilted limb to the flat uplifted area south of it– are displayed. Within the Calders monocline limb, the Bovalar monocline is superimposed. B) Seismic profile CT88-12 and its interpretation. The southern hinge of the Calders monocline is also observed, coinciding with the Bovalar monocline. A vertical tectonic step of at least 0.5s (about 1200m) can be measured between the flat uplifted area and the deepest parts of the tilted limb. C) Contour map of the depth to the base of the Jurassic (in m below the sea level). Some superficial folds are shown for reference, and the trend of the Calders monocline hinges has been traced in a sketch. See Figure 6 for legend and Figure 5 for location. UTM projection (zone 30, coordinates in km), ED50 datum.

evaporites –Prebetics (Ortí, 1973), Basque-Cantabrian Basin (Serrano and Martínez del Olmo, 2004), Parentis Basin (Ferrer *et al*., 2012), Cotiella Basin-Pyrenees (López-Mir, 2015), etc.–in the current study area and in the southern Ebro Basin (Butillé *et al*., 2012), the Middle Muschelkalk evaporitic unit is the only salt unit that experienced some salt flow, as previously indicated by Bartrina and Hernández (1990).

Keuper seismic reflectors onlapping the folded Upper Muschelkalk were identified in the two limbs of the Monchén salt anticline, located North of the Monchén basement high (Figs. 9B, C; 10A). This fold coincides with and is included in the Mirambell anticline core, and affects the whole Mesozoic cover and the basement. However, in the seismic profile CT88-16 (Fig. 9B), the anticline folding the supra-salt cover is tighter in the Upper Muschelkalk than in the Jurassic, so that by flattening the base of the Jurassic, the Keuper reflectors become subhorizontal, onlapping the Upper Muschelkalk that remains folded. Therefore, two folding phases occurred: the first during the sedimentation of the Keuper and the second during the Cenozoic contraction.

The interpreted Keuper growth strata over the Upper Muschelkalk drape fold in the seismic profile CT88-17 (Fig. 9C) and the parallel Keuper reflectors onlapping the salt-cored anticline (Monchén salt anticline) indicate that the Upper Muschelkalk anticline developed by migration of the Middle Muschelkalk salt towards its core. This took place before and during deposition of the Keuper, beneath an overburden of 130-160m of Upper Muschelkalk carbonate rocks. The salt weld over the Monchén basement high can be interpreted as the result of sideways salt migration from above the basement high, accumulating and generating the Monchén salt anticline (Fig. 9).

The salt flow could have been triggered by the resumed activity of the high-angle normal faults during the Late Triassic, while the Keuper facies was being deposited. This activity forced the development of drape folds in the Upper Muschelkalk, observed in CT88-15 and CT88-17 seismic profiles (Figs. 8A, 9C). The Keuper sediments were deposited filling the relief that was being generated by the folding of the Upper Muschelkalk. The differential load exerted by the Keuper sediments could also have enhanced the Middle Muschelkalk salt flow.

Conversely, in the southern Ebro Basin, while salt structures also mainly consist of the Middle Muschelkalk salt unit, they developed during the Early Cretaceous rifting event (Butillé *et al*., 2012).

## MESOZOIC EXTENSIONAL STRUCTURE DEVELOPED DURING THE JURASSIC TO EARLY CRETACEOUS RIFTING EVENT

The Maestrat Basin experienced a second rifting event during the Late Jurassic and Early Cretaceous. We analyzed this event to determine the configuration of the basin and the extensional structures bounding it.

### Jurassic

#### *Jurassic thickness variations*

Jurassic thickness variations are difficult to establish in the seismic profiles, as the base of the syn-rift Malm unit cannot be clearly identified. Field measurements of the syn-rift Jurassic thicknesses are also scarce because its base hardly crops out in the area studied. The interpretation of the wells (located in Fig. 2) by Martínez-Abad (1991) shows that the greatest thickness variations within the Jurassic units are located in the Lower Lias units (Cortes de Tajuña and Cuevas Labradas Fms.). Although these units are commonly interpreted as the post-rift of the Triassic rifting, in the study area they vary from about 135m in the Bovalar-1 and Bovalar-2 wells, to 300m in the Maestrazgo-2 well (towards the SW) and 585m in the Mirambell-1 well (towards the NW, with the Anhydrite zone at its base). The Ablanquejo Group (Upper Lias) and the Chelva Fm. (Dogger) have gentle thickness variations. The first thickens towards ENE, from 54m in the Maestrazgo-2 well and 67m in the Mirambell-1 well, to 105m in the Bovalar-1 well. Conversely, the Chelva Fm. (Dogger) thickens gently towards SSE, from 63m in the Mirambell-1 well to 93m in the Bovalar-1 well and 116m in the Maestrazgo-2 well. The Iàtova Fm. (Lower Malm) presents a nearly constant thickness (about 25m), while the other Malm units (Polpís-Ascla and Bovalar-Pleta fms.) gently thicken towards ESE, from 407m (Mirambell-1) to 490m (Maestrazgo-2) and to more than 650m in the Bovalar anticline, (deduced from combining the wells (Bovalar-1 and 2) and field data).

#### *Interpretation of the basin evolution during the Jurassic*

In view of the thickness variations, some extension is needed during the Lias, which would be a consequence of the Hettangian-Lower Pliensbachian rifting event controlled by listric normal faults (Aurell *et al*., 1992; Roca and Guimerà, 1992; San Roman and Aurell, 1992; Roca *et al*., 1994); although in other parts of the Iberian rift system the Cortes de Tajuña Fm. has also been related to evaporite solution, collapse and breccia formation (Yébenes, 1973; Giner, 1980).

The Iàtova Fm. (Lower Malm) is considered the last pre-rift Malm (Salas *et al*., 2001). Regarding the other Malm units, the major thickness variations are found when comparing the
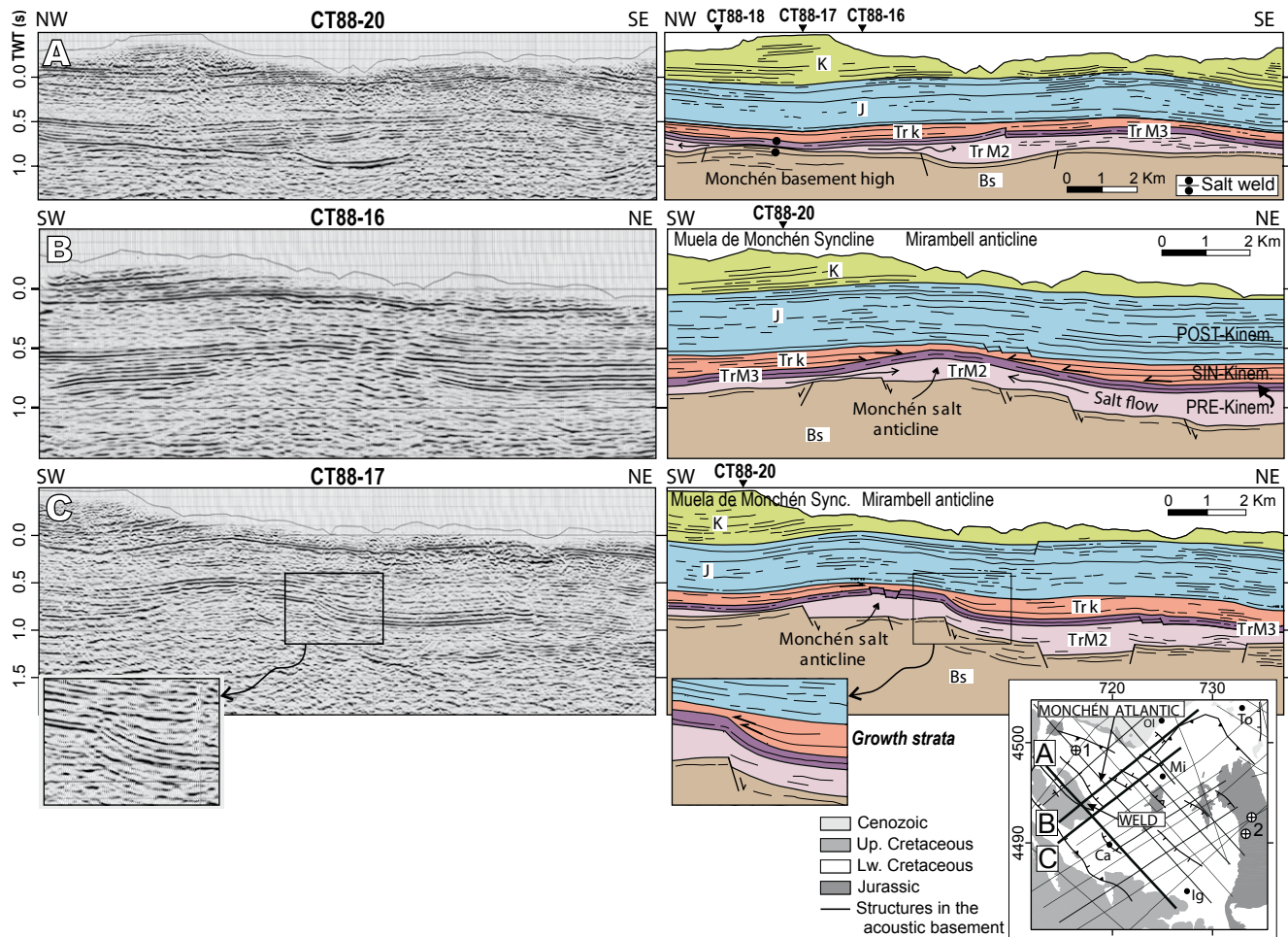
**FIGURE 9.** Seismic profiles A) CT88-20, B) CT88-16 and C) CT88-17 and their interpretation. A) A salt weld is observed over the Monchén basement high. The Middle Muschelkalk thickness variations are thus displayed. B) The Monchén salt anticline developed N of the Monchén basement high is shown, being the Keuper reflectors onlapping the folded Upper Muschelkalk. C) A drape fold of the Upper Muschelkalk forced by the resumed extensional activity of high-angle normal faults in the acoustic basement during the Late Triassic is shown. Some growth-strata in the Keuper reflectors are deduced, indicating that it was deposited during the extension. See location in Figure 5, and Figure 6 for legend.

thicknesses in the study area from 407m to more than 650m, with those in the adjacent area of Albarracín, about 250-270m (Hernández, 1985). Therefore, a larger area has to be considered to characterize the major thickness variations for the Malm, suggesting that the Jurassic boundaries of the basin probably do not coincide with the Lower Cretaceous ones.

**Lower Cretaceous**

*Lower Cretaceous thickness variations and extensional structure*

Lower Cretaceous thicknesses were obtained from field data, cross-sections, wells, and from Salas (1987). As previously explained, the Valanginian to Hauterivian rocks are only present in the eastern part of the study area: E of the Bovalar anticline and S of the Turmell fault, and mostly S of the Xert fault. The Barremian and Aptian thickness

distributions show the presence of different scale normal faults. The major ones are the Villarluengo fault, Bordón fault, Ortells fault and Xert fault (Figs. 2; 11D-D').

The western normal fault is the Villarluengo fault (Fig. 12): an E-W-trending, S-dipping non-inverted Mesozoic normal fault, which brings Lower Cretaceous rocks in its hanging wall into contact with Jurassic rocks in its footwall. The Escucha Fm. (of Albian age) overlies the fault, indicating that it was active before its sedimentation.

The Bordón fault (Fig. 11D-D'), a NE-SW-trending, SE-dipping normal fault, separates 1100m of Barremian and Aptian rocks in its hanging wall (S) from about 365m in its footwall (N), in the surroundings of Ladruñán village (Canérot, 1974), about 6km to the North. Just North of the Bordón fault, about 150-200m of Barremian
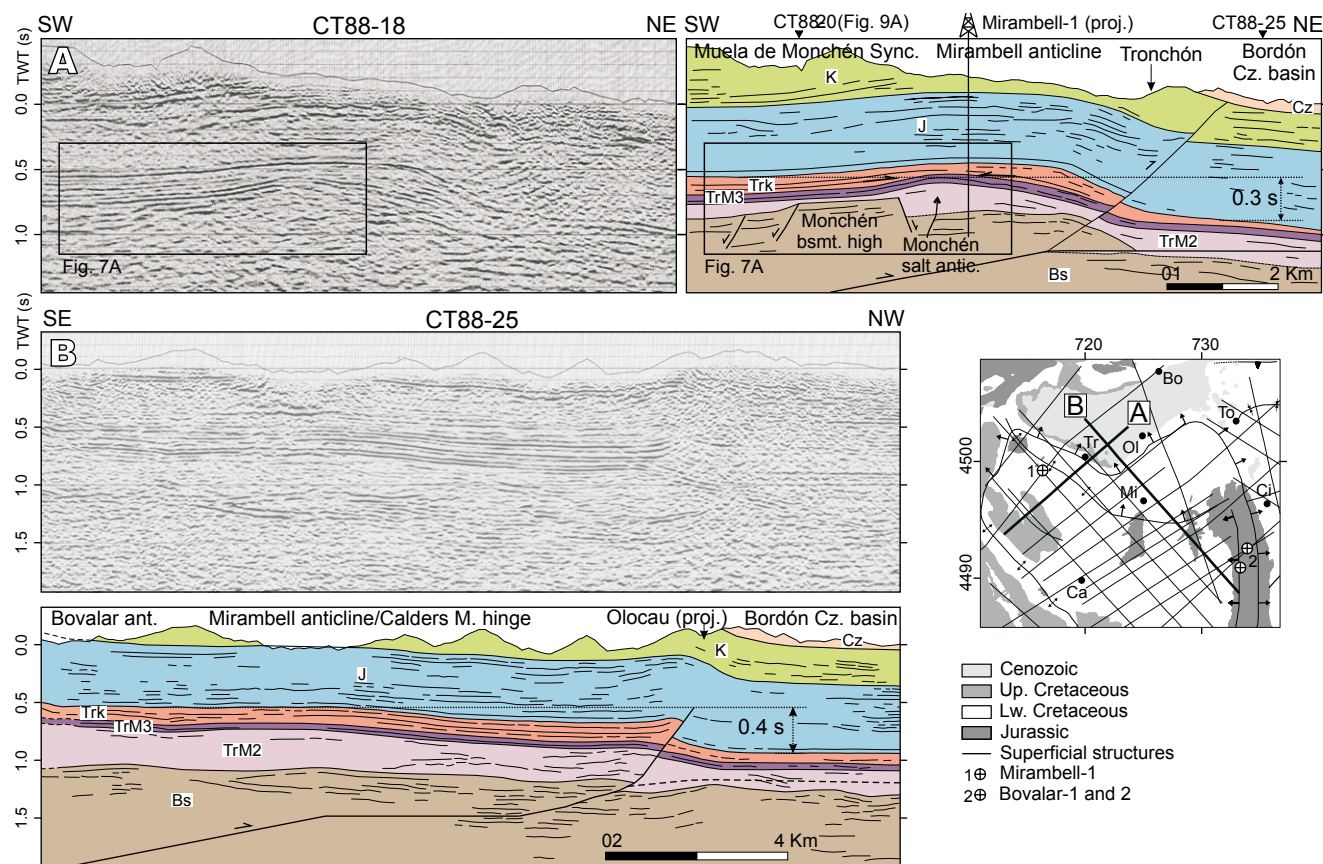
**FIGURE 10.** A) Seismic profile CT88-18 and its interpretation. A vertical tectonic step of 0.3s (about 800m) is deduced between the base of the Jurassic in the Muela Monchén syncline and below the Cenozoic Bordón Basin. See Figure 7A for a detail of the Keuper reflectors onlapping the folded Upper Muschelkalk. B) Seismic profile CT88-25 and its interpretation. The Calders monocline limb and its southern hinge are observed. A vertical tectonic step of 0.4s (about 1000m) is measured comparing the base of the Jurassic. See Figure 6 for legend.

rocks can be measured in a Cenozoic-cored syncline located in the footwall of the fault and attached to it. This Barremian thickness is similar to that measured in the Ladruñán sequence (about 190m of Barremian rocks), where the entire Aptian-Barremian succession is preserved. Comparing these Barremian thicknesses (150-200m) in the footwall of the fault with those measured in the Bordón anticline (more than 600m), located in the hanging wall of the fault, it can be ascertained that these thickness variations are related to the Bordón fault. Eastwards, the Paleogene alluvial rocks overlie the Bordón fault (Fig. 4). The lowest Cenozoic units are folded but not faulted. These folds are interpreted as being produced by the eastern continuation of the Bordón fault as a blind fault for about 7km. As no significant differences in the Barremian and Aptian sequences can be observed N and S of this blind fault segment, this is interpreted to be a newly formed thrust in this area, which grew during the Cenozoic contraction as a lateral continuation of the inverted normal fault. The Upper Cenozoic units unconformably overlie the folded Lower Cenozoic units (Fig. 4).

Towards the E, and located in a more internal position, the E-W-trending, S-dipping Ortells fault separates Barremian sequences of about 750m, in its hanging wall, from sequences of 570m in its footwall.

East of the area studied, more than 2.5km of Lower Cretaceous rocks are found in the downthrown hanging wall of the Xert fault, which is the depocenter of the Salzedella sub-basin, while in its footwall only about 1000m of Lower Cretaceous can be measured (Salas, 1987). The Xert fault (Fig. 4) is an E-W-trending, S-dipping normal fault of listric geometry, as deduced from the rollover geometry preserved in the Lower Aptian units in its hanging wall (Salas *et al.*, 1995). A listric normal fault has also been interpreted from seismic profiles (Antolín-Tomás *et al.*, 2007), which is probably the eastern continuation of the Xert fault.

In the southern limb of the Tarayuela anticline, a normal fault is deduced, the Tarayuela fault (Fig. 11), parallel to the fold trend (Fig. 4). It separates sequences of 380 and 350m of Barremian and Aptian rocks in its hanging wall (Tarayuela anticline–southwest of Cantavieja–and the
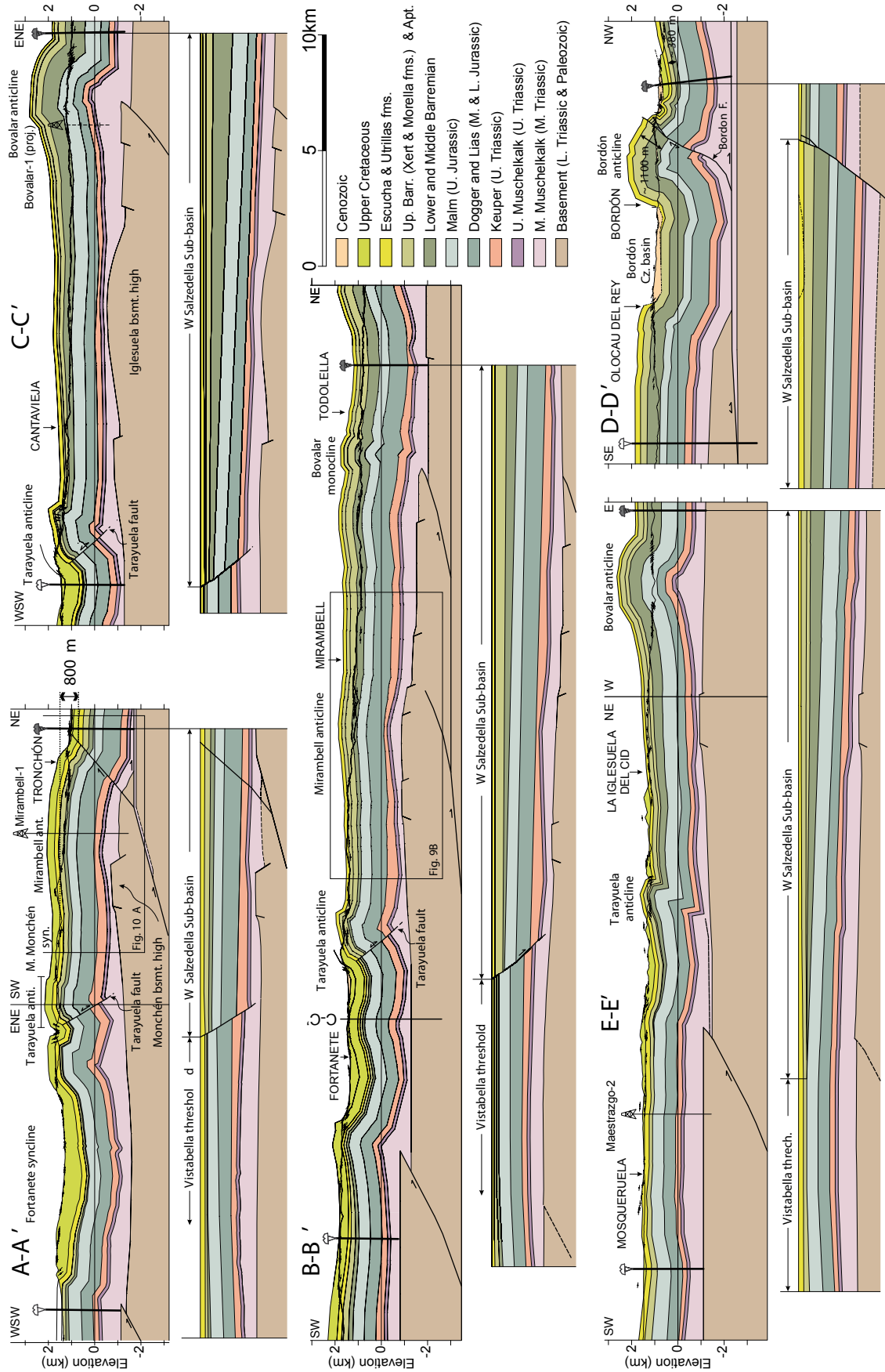
**FIGURE 11.** Balanced cross-sections of the studied area. The deformed and the unfolded sections at the end of the Late Jurassic-Early Cretaceous rifting are shown. Unfolded cross-sections are only drawn between the pin and the loose lines. See Figures 4 and 5 for location. A-A': a tectonic vertical step of 800m is measured comparing the elevation of the base of the Upper Cretaceous in the Muela de Monchén syncline (1500m a.s.l.) and the same level under the Cenozoic Bordón Basin (700m a.s.l.), the same vertical step that González *et al.* (1998) described comparing the base of the Utrillas Fm.

western part of the Mirambell anticline), from 150 and 180m in its footwall (Maestrazgo-2 well and eastern limb of the Cañada de Benatanduz anticline) (Fig. 4).

The Lower Cretaceous sequence in the Maestrazgo-2 well is 350m thick, including 200m of the Escucha and Utrillas fms. and 150m of the Upper Aptian formations (Villarroya de los Pinares and Benassal) which directly overlie the Bovalar Fm. (Malm) (Martínez-Abad, 1991). These Lower Cretaceous sequences decrease towards the SE and in the surroundings of Vistabella only 100m of Aptian rocks and a few meters of Escucha and Utrillas Fms. overlie the Polpís Fm. (Lower Kimmeridgian). In turn, the Polpís Fm. directly overlies the Triassic rocks (Canérot, 1974).

NW-SE-trending and mostly SW-dipping normal faults of metric slips are observed in the Mirambell and Tarayuela anticlines, affecting the Lower Cretaceous units. In the hanging wall of the Villarluengo normal fault, E-W-trending, S-dipping normal faults with metric slips are also observed (Fig. 12). These minor faults were also observed in other areas of the Maestrat Basin (in the Galve sub-basin; Liesa *et al.*, 2006) leading to the changes in thickness in the Lower Cretaceous units.

### Main tectonostratigraphic domains and interpretation of basin evolution during the Lower Cretaceous rifting

Considering the thickness distribution of the Barremian and Aptian rocks, the study area partially comprises two of the principal paleogeographic units of the Maestrat Basin: the western part of the Salzedella sub-basin and the Vistabella threshold (Fig. 2).

i) Western Salzedella sub-basin. The Barremian and Aptian units progressively thicken towards the N, from the Tarayuela anticline (400m) to the Bordón anticline (about 1100m) (Fig. 11). The normal faults with metric slips probably lead to the northward thickening of the Lower Cretaceous units in the western Salzedella sub-basin. However, these faults were not considered during construction of the cross-sections, as they cannot be represented at that scale. Therefore, the Barremian and Aptian units display a major scale wedge geometry when the cross-sections are unfolded (Fig. 11). Sediments of Valanginian to Hauterivian age could have been eroded or never deposited W of the Bovalar anticline. The northern boundary of the Salzedella sub-basin is composed of different normal fault segments: the Villarluengo fault, Bordón fault, Ortells fault and, located in a more internal position, the Xert fault. In the southern margin of the Salzedella sub-basin the Vistabella threshold is found; which has been interpreted as the high block developed by the rollover folding in the hanging wall of the Mesozoic

extensional fault system that formed the Salzedella sub-basin (Fig. 2) (Salas and Guimerà, 1996; Salas *et al.*, 2005). A NW-SE-trending, NE-dipping normal fault was deduced at this southern boundary (the Tarayuela fault), slightly modifying the geometry of the rollover. To the E, the Tarayuela fault ends and the geometry of the southern margin of the basin is only determined by the rollover geometry (Fig. 11E-E').

ii) Vistabella threshold. It is located S and W of the Salzedella sub-basin separating it from the Penyagolosa and the Galve sub-basins (Fig. 2). It was an elevated area containing only local remains of Lias and Dogger rocks, incomplete Upper Jurassic –overlying the Triassic rocks– and reduced Lower Cretaceous sequences. Therefore, deposition was poor at the Vistabella threshold, while some units were partially or totally eroded.

## CENOZOIC CONTRACTIONAL STRUCTURE

As explained above, the inversion of the Maestrat Basin generated a wide uplifted area as a result of the uplifting of the hanging wall of the Maestrat basement thrust. In the area studied, this uplifted area includes the Calders monocline on its northern margin, which narrows laterally and is modified in its central part by the N-S-trending Bovalar anticline (Fig. 13).

### Structure of the uplifted area south of the Calders monocline hinge

In its eastern part, the uplifted area (Fig. 13) includes a flat-lying region; while the western part is characterized by a system of large folds that involve the supra-salt cover–although some are rooted in the basement (Mirambell anticline). They are more than 10km long and have wavelengths of about 5km (Fig. 11). Their main orientation is NW-SE (Fig. 4) and to the North some folds progressively adopt a NNE-SSW trend (the Cuarto Pelado syncline and Tarayuela anticline). The Tarayuela anticline becomes a W-verging monocline in its NNE-SSW-trending segment, which generates a vertical tectonic step of 450m within the uplifted area, related to the inversion of the Tarayuela basement fault (Figs. 8C; 13). The formation of the S-verging Tarayuela anticline during the Cenozoic contraction could also have been triggered by the inversion of this normal fault, folding the Mesozoic cover without cutting the Upper Cretaceous rocks (Fig. 11A-A', B-B', C-C').

### The Calders monocline

The Calders monocline hinge is located North of the Muixacre Mountain in the area E of the Bovalar anticline,
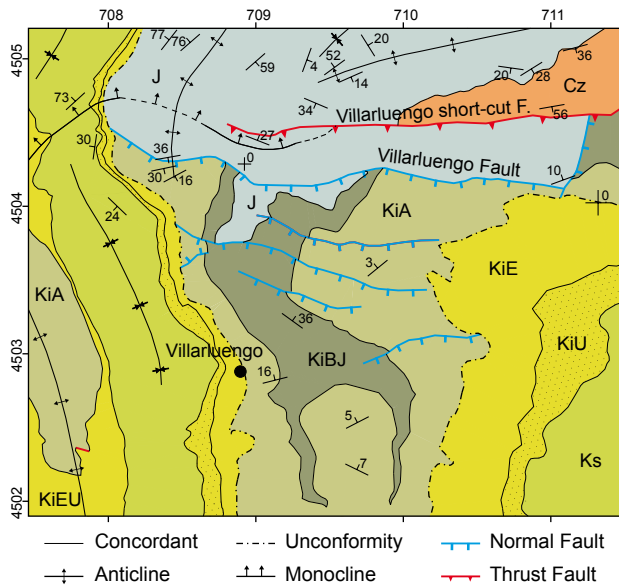
**FIGURE 12.** Detailed geological map of the Villarluengo normal fault and its short-cut thrust, located to the N. See location in Figure 4. Abreviations: Cz= Cenozoic, Ks= Upper Cretaceous, KiU= Utrillas Fm. (Late Albian), KiE= Escucha Fm. (Early and Middle Albian), KiA= Aptian, KiBJ= Barremian and Jurassic in Purbeck facies, J= Jurassic. The Villarluengo normal fault puts in contact the Lower Cretaceous units in the hanging wall with the Malm in the footwall, indicating that it was active during the Late Jurassic-Early Cretaceous rifting event. The Escucha Fm. covers the fault. Zone 30 UTM coordinates (km), datum ED50.

and south of Mirambell in the area W of the Bovalar anticline (Fig. 13).

W of the Bovalar anticline, the asymmetric NW-SE-trending Mirambell anticline is the continuation of the Calders Monocline (Fig. 4), which is above a vertical tectonic step of 800m – 0.3s (Figs. 10A; 11A-A'). Its northward tilted limb is divided into two dip domains: the southern, wider one (3-15N) and the steeply dipping northern one (25-70N) (Figs. 4; 11A-A'; 13). The Mirambell anticline frontal limb widens towards the E, and changes its trend to NE-SW (Fig. 13) SW of Olocau, where it is also divided into two dip domains. A vertical tectonic step of 0.4s (about 1000m) is measured in its limb (Fig. 10B).

Parallel to this frontal limb, there is the synformal flexion that constitutes the southern boundary of the Cenozoic Bordón Basin, trending NW-SE to NE-SW. This synformal flexion is the eastern continuation of the Morella syncline, mostly oriented WNW-ESE (Figs. 7; 8; 13). These synformal structures are the northern synformal hinge of the Calders monocline (Fig. 13), and also constitute the northern limit of the uplifted area.

N of the Calders monocline a synformal area appears (dashed synformal structures in Fig. 13), giving rise to

the Cenozoic Bordón Basin. This is filled with flat-lying terrigenous sediments (González, 1989), which onlap the Upper Cretaceous rocks of its steeply dipping southern boundary and are accordingly gently deformed with it. This Cenozoic basin disappears towards the E, being thrust by the Ortells fault, which is the southern boundary of the Cenozoic basin in this eastern part. North of the Morella anticline, this synformal area reappears –partially filled with Cenozoic rocks– and continues towards the E in the footwall of the Turmell fault.

In the eastern part of the Calders monocline, the Ortells and Morella anticlines appear between the northern synformal hinge of the monocline, and the synformal area found N of it (dashed synformal structures in Fig. 13). The NW-SE-trending Morella anticline and E-W-trending Ortells anticline are located in the hanging wall of S-dipping thrusts, with the fault associated with the Ortells anticline cropping out in the inverted Ortells fault (Figs. 4; 7C; 13). These structures relay laterally, as they have in common the NE limb of the Morella syncline (Figs. 4; 13).

**Structures within the Calders monocline frontal limb**

The Calders monocline frontal limb is modified in its central part by the N-S-trending Bovalar anticline (Figs. 4; 8). Two segments can be differentiated: a northern NNW-SSE-trending, ENE-verging monoclinal segment –between La Todolella and Cinctorres– and a southern NNW-SSE to N-S-trending box-fold anticline (Figs. 4; 13).

Seismic profile CT88-15 (Fig. 8A) shows the Calders monocline hinge at the eastern continuation of the Mirambell anticline, with the Bovalar monocline located within the tilted limb of the Calders monocline. Conversely, in seismic profile CT88-12 (Fig. 8B) the Calders monocline hinge coincides with the Bovalar monocline. Towards the S, the Bovalar monocline evolves into a box-fold anticline, near Cinctorres, which also has its western limb more elevated than the eastern one (Figs. 7C; 11C-C'). South of the Bovalar-2 well, this vertical tectonic step disappears and both limbs of the anticline are at the same elevation (Fig. 11E-E'), located within the flat uplifted limb of the Calders monocline (Fig. 13).

The widest part of the Calders monocline limb is located in its central part, where a vertical tectonic step of 0.5s (about 1200m) was measured (Fig. 8). Towards the E, this tilted limb becomes narrower, as the Morella syncline and the monocline southern hinge converge; and the E-W-trending, N-verging Turmell fault (the direct outcrop of the Maestrat basement thrust) is found
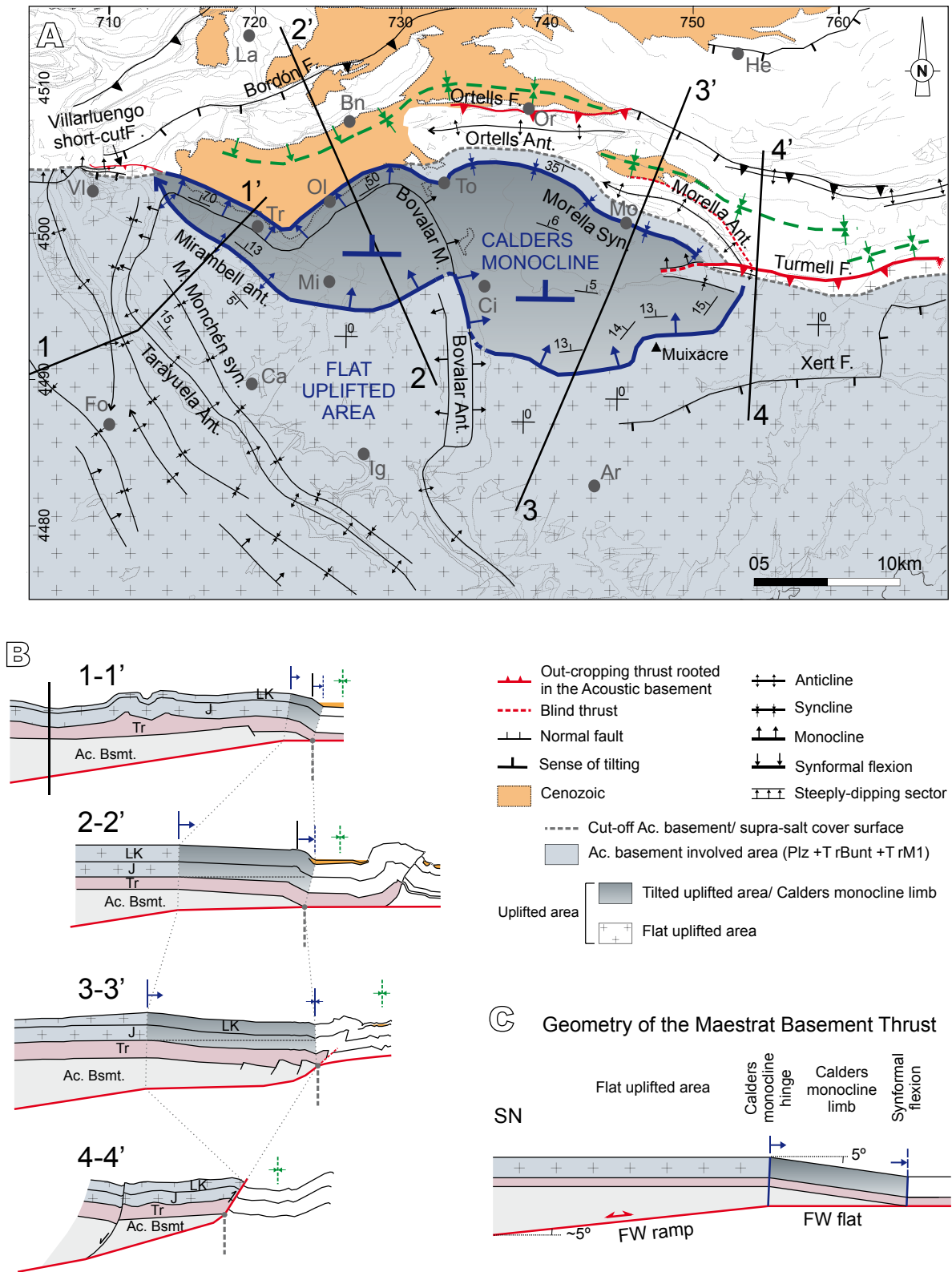
**FIGURE 13.** A) Structural map showing the major structures of the area studied and the location of schematic cross-sections (UTM projection (zone 30, coordinates in km), ED50 datum). B) Schematic cross-sections showing the lateral evolution of the Calders monocline. 1-1': based on cross-section A-A' (Fig. 11). 2-2': based on cross-section D-D' (Fig. 11) and seismic profile CT88-25 (Fig. 10B). 3-3': modified after an unpublished cross-section from Guimerà. 4-4': modified after cross-section XV in Guimerà (1988). C) Idealized cross-section showing the geometry of the Maestrat basement thrust deduced from the fold-bend fold (Calders monocline) observed at the surface.

to the E (Fig. 13). Its hanging wall is uplifted, resulting in a fault throw of about 800m. The Turmell fault cuts across the Calders monocline limb, continuing as a blind thrust for about 4km more, and at surface is an E-W-trending, N-verging monocline.

Towards the W, the Calders monocline also narrows, disappearing in the hanging wall of the E-W-trending, S-dipping Villarluengo short-cut thrust (Figs. 12; 13). This short-cut thrust continues towards the W as a blind thrust, which is expressed at surface as an E-W-trending, N-verging monocline (Fig. 13) that continues up to the southern and western margins of the Aliaga Cenozoic Basin (González and Guimerà, 1993; Guimerà and Salas, 1996). Therefore, the Calders monocline becomes narrower laterally while the associated vertical tectonic step also decreases from 0.5s (about 1200m) measured in its widest central part, towards the E and W (0.3s: 800m).

## DISCUSSION

Summing up, the inversion of the Salzedella sub-basin generated a wide uplifted area (more than 3600km²), bounded to the North by a vertical tectonic step of 800 to 1200m. This uplifted area is interpreted as the result of the inversion of the lower segment (within the acoustic basement) of the Mesozoic extensional fault system that generated the Salzedella sub-basin. This inverted fault is the Maestrat basement thrust, which extends from the southern boundary of the Aliaga Cenozoic Basin to the eastern limit of the Turmell fault. The surface expression of the Maestrat basement thrust is the Calders monocline in its central part. Towards the E and W of the Calders monocline, the Turmell and Villarluengo short-cut thrusts developed.

No Mesozoic thickness variations can be identified between the hanging wall and footwall of the Turmell fault, which is interpreted as a short-cut of the E-W-trending, S-dipping Xert listric normal fault located south of it (Fig. 13). The Xert fault, which has a rollover geometry preserved in its hanging wall (Salas and Guimerà, 1996), was only inverted in its lower segment within the acoustic basement; while in the upper segment, the short-cut–Turmell fault–developed (Fig. 13B, 4-4'). On the western side of the Calders monocline, the Villarluengo short-cut thrust is the result of the inversion of the Mesozoic Villarluengo normal fault (Fig. 12) which, similarly to the Xert fault, was also inverted in its lower segment. A short-cut containing in its hanging wall the non-inverted segment of the normal fault developed within its footwall (Fig. 12).

### Interpretation of the Calders monocline

The Calders monocline is interpreted as a fault-bend fold that developed as the rising hanging wall adapted to the flat-ramp-flat geometry deduced for the Maestrat basement thrust (Fig. 13C). The wide extension of the uplifted area, which is maintained elevated for about 40km towards the S, and the low-angle dip (~5°) of the Calders monocline limb imply that the Maestrat basement thrust ramp has a very low-angle dip, and is rooted in the upper crust. This interpretation is in holding with Seillé et al. (2015) who suggested, after the interpretation of wide-angle seismic, magnetotelluric (MT) and gravity data, that the Cenozoic thickening in the Iberian Chain is concentrated in the upper crust, thereby coinciding with Guimerà and Álvaro (1990).

Assuming this low-dip geometry for the Maestrat basement thrust (Fig. 13C), the flat uplifted area is located above the footwall ramp of the Maestrat basement thrust, while the transition from ramp to flat is reflected at surface by the southern hinge of the Calders monocline. The monocline limb is above the hanging wall ramp and the footwall flat, and its width depends on the amount of displacement above the footwall flat. Therefore, the different orientations of the southern hinge of the Calders monocline show the orientation changes of the Maestrat basement thrust ramp, which is the result of the inversion of previous Mesozoic extensional fault segments with the same orientations.

### Cut-off line of the acoustic basement in the hanging wall of the Maestrat basement thrust

In the area located west of the Bovalar anticline, the cut-off of the acoustic basement is located below the synformal flexion that constitutes the southern boundary of the Cenozoic Bordón Basin (Figs. 10; 11A-A'; 13). East of the Bovalar anticline, the cut-off of the acoustic basement coincides with the Morella syncline (Fig. 13). In this area, the Ortells and Morella thrusts–rooted in the Maestrat basement thrust–modified this synformal frontal flexion. Further E, this cut-off line is located in the hanging wall of the Turmell fault; while to the W, it is located in the hanging wall of the Villarluengo short-cut thrust.

### Structures within the Calders monocline frontal limb: the Bovalar anticline

The NNW-SSE-trending Bovalar monocline is located within the Calders monocline limb, and modifies its geometry. The formation of the Bovalar

anticline and its northern monoclinal segment should be related to a NW-SE-trending basement thrust, at least in its northern part, where a vertical tectonic step is observed between the limbs of the anticline (Figs. 7C; 11C-C'). The origin of this thrust could be related to the inversion of previous Triassic normal faults. As shown in Figure 8B, some NW-SE-trending, SW-dipping Triassic normal faults where interpreted as bounding to the NE the Middle Muschelkalk accumulation located N of the Iglesuela basement high. Towards the S–below the N-S-trending, southern segment of the Bovalar anticline–this thrust probably terminates, as no vertical tectonic step can be identified (Fig. 11E-E'). Conversely, the superficial structure developed above it–the N-S-trending box-fold anticline–continues southwards for more than 8km as a salt-cored detachment fold. The thick Middle Muschelkalk originally deposited in that area (Fig. 7B, E) could have favored the development of this salt-cored fold as a continuation of the northern monocline, and its progression southwards beyond the termination of the acoustic basement thrust.

The Bovalar monocline and the basement thrust below it link to the NE-SW-trending steeply-dipping domain of the Calders monocline limb in the surroundings of Olocau. The seismic profiles also show that a thrust rooted in the Maestrat basement thrust cuts this steeply-dipping part of the monocline, both in the NE-SW Olocau sector and in the NW-SE Tronchón sector (Fig. 10), probably related to the inversion of Mesozoic normal faults with those orientations, making the steeply dipping domain more pronounced.

### Middle Muschelkalk detachment level and salt-related structures developed during contraction

As mentioned above, the Middle Muschelkalk evaporitic unit played an important role during the Cenozoic contraction, by decoupling the acoustic basement and the supra-salt cover. During contraction, the basement was faulted while the supra-salt cover was folded and thrust, and adapted to the geometry of the basement structures. During the Cenozoic contraction, the last changes in the distribution of the Middle Muschelkalk salt resulted in its current distribution, due to the folding of the supra-salt cover. Previous salt structures were amplified (Monchén salt anticline) while new box-fold, salt-cored, anticlines developed (Bovalar, Tarayuela, and Cañada de Benatanduz anticlines; Figs. 4; 7E; 11). The Mesozoic cover was folded, detached in the Middle Muschelkalk evaporites, which flowed towards the lower-pressure cores of the rising anticlines, developing elongated salt accumulations (Fig. 7E).

### Orientation of structures

As described, the main orientation of the Cenozoic contractional structures within the study area is mostly WNW-ESE; although they can vary to E-W and to N-S. Unlike other areas of the Maestrat Basin and the Iberian Chain, where superposition of structures generated in successive deformation events is clear –i.e., within and North of the Aliaga Cenozoic Basin (Simón, 1980; Guimerà, 1988)– in the study area no superposition of this kind is observed. For this reason, the differently oriented structures are considered to be synchronous, resulting from the inversion of a complex system of previous Mesozoic extensional faults with different orientations, which resulted in the formation of thrusts and folds which change their orientation. The heterogeneous distribution of the detachment level (Middle Muschelkalk), which resulted from the distribution of horsts and grabens in the acoustic basement, and influenced the development of contractional structures, also has to be taken into account.

### CONCLUSIONS

During the Late Permian-Late Triassic rifting, a system of high-angle normal faults developed in the present-day acoustic basement. These faults define a system of horsts, grabens and half-grabens, involving the Upper Permian to the Middle Muschelkalk units, which were filled and overlain by the Middle Muschelkalk evaporitic facies deposited during the extension. As a result, depositional thickness variations within the Middle Muschelkalk appeared, which were enhanced by salt flow during the Late Triassic due to the resumed activity of normal faults in the basement. This is deduced from the growth strata in the Keuper seismic reflectors, which onlap the Upper Muschelkalk folds. The last thickness variations within the Middle Muschelkalk were generated during the Cenozoic contraction, as the Mesozoic salt structures were amplified and new salt-cored detachment folds developed.

Although widely considered as the Triassic post-rift, some extension is needed during the Early Lias, as thickness variations of the units of this age are identified after comparison of thicknesses in exploration wells. During the Late Jurassic–Early Cretaceous rifting event, the Maestrat Basin developed, and within it, the Salzedella sub-basin, bounded to the N by the Villarluengo, Bordón, Ortells and Xert faults. These faults separate the Barremian and Aptian sequences of up to 1100-2500m in their hanging walls from sequences of about 400m in their footwalls. Within the basin, minor normal faults of metric slips probably resulted in the progressively northward thickening of the Salzedella sub-basin.

During the Cenozoic contraction, the Salzedella sub-basin was inverted. Its North-bounding normal fault system was inverted, at least in its lower segment within the acoustic basement (Maestrat basement thrust). A wide uplifted area developed in its raised hanging wall. This uplifted area is bounded to the N by the E-W-trending, N-verging Calders monocline, which is the surface expression of the Maestrat basement thrust. Laterally, the Calders monocline terminates and links to the outcropping Maestrat basement thrust in the Turmell and Villarluengo thrusts, which are short-cuts of the inverted Xert and Villarluengo Mesozoic normal faults.

The Calders monocline is interpreted as a fault-bend fold, indicating a flat-ramp-flat geometry of the Maestrat basement thrust, with the southern hinge of the Calders monocline being the superficial expression of the transition from ramp to flat in the basement thrust. The cut-off line of the acoustic basement in the hanging wall of the Maestrat basement thrust coincides with the northern synformal hinge of the Calders monocline, located at the southern boundary of the Bordón Cenozoic Basin and in the Morella syncline. The frontal tilted limb of the Calders monocline has a maximum width of about 13km and narrows laterally, linking to direct outcrops of the Maestrat basement thrust (Turmell and Villarluengo short-cut thrusts). In these two areas, the cut-off line of the acoustic basement is found in the hanging walls of the basement thrusts. This cut-off line makes the transition from thick-skin to thin-skin areas.

The monocline geometry is modified in its central part by the N-S trending Bovalar anticline, originated by the inversion of a previous Triassic normal fault and the presence of a thick Middle Muschelkalk evaporitic unit originally deposited in its hanging wall.

The uplifted hanging wall of the Maestrat basement thrust remains elevated for about 40km to the S, and the frontal limb of the Calders monocline dips about 5° towards the N. These observations indicate that a very low-angle ramp is needed for the Maestrat basement thrust ramp, rooted in the upper crust.

Mesozoic extensional structures with different orientations, together with a thick Middle Muschelkalk evaporitic unit, played an important role in the formation of the Cenozoic contractional structures, affecting their location and orientation, and the different deformation styles between the acoustic basement and the supra-salt cover. The acoustic basement was mainly faulted while the supra-salt cover was mainly folded and thrust, adapting to the basement structures.

## ACKNOWLEDGMENTS

## REFERENCES

Almera, J., Anadón, P., Godoy, A., 1982. Mora de Rubielos, sheet 591. Mapa Geológico de España 1:50.000. Madrid, Servicio de Publicaciones, Ministerio de Industria y Energía, 2ª Serie, 1ª Edición.

Álvaro, M., Capote, R., Vegas, R., 1979. Un Modelo de evolución geotectónica para la cadena Celtibérica. Acta Geológica Hispánica, 14, 172-181.

Antolín-Tomás, B., Liesa, C.L., Casas, A.M., Gil-Peña, I., 2007. Geometry of fracturing linked to extension and basin formation in the Maestrazgo basin (Eastern Iberian Chain, Spain). Revista de la Sociedad Geológica de España, 20 (3-4), 351-365.

Archivo Técnico de Hidrocarburos. Ministerio de Industria, Energía y Turismo, Spain. Available at https://geoportal. minetur.gob.es/ATHv2/welcome.do (accessed 13 April 2016).

Aurell, M., Meléndez, A., San Román, J., Guimerà, J., Roca, E., Salas, R., Alonso, A., Mas, R., 1992. Tectónica sinsedimentaria distensiva en el límite Triásico-Jurásico en la cordillera ibérica. Actas del III Congreso Geológico de España, 1, 50-54.

Bartrina, T., Hernández, E., 1990. Las unidades evaporíticas del Triásico del subsuelo del Maestrazgo. In: Ortí, F., Salvany, J.M. (eds.). Formaciones evaporíticas de la Cuenca del Ebro y cadenas periféricas, y de la zona de Levante. Nuevas aportaciones y guía de superficie. Barcelona, Empresa Nacional de Residuos Radiactivos (ENRESA) i Universitat de Barcelona (UB, Departament de Geoquímica, Petrologia i Prospecció Geològica), 34-38.

Bover-Arnal, T., Moreno-Bedmar, J.A., Frijia, G., Pacual-Cebrian, E., Salas, R., 2016. Chronostratigraphy of the Barremian-Early Albian of the Maestrat Basin (E Iberian Peninsula): integrating strontium-isotope stratigraphy and ammonoid biostratigraphy. Newsletters on Stratigraphy, 49 (1), 41-68. DOI: 10.1127/nos/2016/0072

Butillé, M., Ferrer, O., Granado, P., Roca, E., Muñoz, J.A., Ballesteros, J.C., Giménez, A., Vallejo, R.A., González, P., 2012. Evidencias de deformaciones salinas en las sucesiones mesozoicas del sector sur de la Cuenca del Ebro. In: Fernández, L.P., Fernández, A., Cuesta, A., Bahamonde, J.R. (eds.). Oviedo, VIII Congreso Geológico de España. Geo-Temas, 13, 176.

Campos, S., Aurell, M., Casas, A., 1996. Origen de las brechas de la base del Jurásico en Morata de Jalón (Zaragoza). Geogaceta, 20 (4), 887-889.

Canérot, J., 1974. Recherches géologiques aux confins des chaînes ibérique et catalane (Espagne). PhD Thesis. Université Paul Sabatier, Toulouse, 517pp.

Canérot, J., Leyva, F., 1972. Peñarroya de Tastavins, sheet 520. Mapa Geológico de España 1:50.000. Madrid, Servicio de Publicaciones, Ministerio de Industria y Energía, 2ª Serie. 1ª Edición.

Canérot, J., Pignatelli-García, R., 1972. Aguaviva, sheet 519. Mapa Geológico de España 1:50.000. Madrid, Servicio de Publicaciones, Ministerio de Industria y Energía, 2ª Serie, 1ª Edición.

Canérot, J., Pignatelli-García, R., 1977. Mosqueruela, sheet 569. Mapa Geológico de España 1:50.000. Madrid, Servicio de Publicaciones, Ministerio de Industria y Energía, 2ª Serie, 1ª Edición.

Canérot, J., Crespo-Zamorano, A., Navarro-Vázquez, D., 1977. Montalbán, sheet 518. Mapa Geológico de España 1:50.000. Madrid, Servicio de Publicaciones, Ministerio de Industria y Energía, 2ª Serie, 1ª Edición.

Canérot, J., Cugny, P., Pardo, G., Salas, R., Villena, J., 1982. Ibérica Central- Maestrazgo. In: Dpto. de Estratigrafía de la Facultad de Ciencias Geológicas de la Universidad Complutense de Madrid, y Alonso, A, Arias, C., García, A., Mas, R., Rincón, R, Vilas, L. del CSIC (eds.). El Cretácico de España. Madrid, 273-344.

Castillo Herrador, F., 1974. Le Trias évaporitique des basins de la Vallée de l'Èbre et de Cuenca. Bulletin de la Société Géologique de France, 16 (6), 666-675.

Escudero-Mozo, M. J., Márquez-Aliaga, A., Goy, A., Martín-Chivelet, J., López-Gómez, J., Márquez, L., Arche, A., Plasencia, P., Pla, C., Marzo, M., Sánchez-Fernández, D., 2015. Middle Triassic carbonate platforms in eastern Iberia: Evolution of their fauna and palaeogeographic significance in the western Tethys. Palaeogeography, Palaeoclimatology, Palaeoecology, 417, 236-260. DOI: 10.1016/j.palaeo.2014.10.041

Esnaola, J.M., Canérot, J., 1972. Albocácer, sheet 570. Mapa Geológico de España 1:50.000. Madrid, Servicio de Publicaciones, Ministerio de Industria y Energía, 2ª Serie, 1ª Edición.

Farran, M., 2008. IMAGE2SEGY: Una aplicación informática para la conversión de imágenes de perfiles sísmicos a ficheros en formato SEG Y. In: Pérez, F.J., Cabrera, M.C. (eds.). Las Palmas de Gran Canaria, VII Congreso Geológico de España. Geo-Temas, 10, 1215-1218.

Fernández, O., 2004. Reconstruction of geological structures in 3D. An example from the Southern Pyrenees. PhD Thesis. University of Barcelona, Barcelona, 321pp.

Ferrer, O., Jackson, M.P.A., Roca, E., Rubinat, M., 2012. Evolution of salt structures during extension and inversion of the Offshore Parentis Basin (Eastern Bay of Biscay). In: Alsop, G.I., Archer, S.G., Hartley, A.J., Grant, N.T., Hodgkinson, R. (eds.). Salt Tectonics, Sediments and Prospectivity. London, Geological Society of London, 363 (Special Publications), 361-379. DOI: 10.1144/SP363.16

Gautier, F., 1978. Alcalà de la Selva, sheet 568. Mapa Geológico de España 1:50.000. Madrid, Servicio de Publicaciones, Ministerio de Industria y Energía, 2ª Serie, 1ª Edición.

Gautier, F., 1979. Villarluengo, sheet 543. Mapa Geológico de España 1:50.000. Madrid, Servicio de Publicaciones, Ministerio de Industria y Energía, 2ª Serie, 1ª Edición.

Gautier, F., Barnolas, A., 1979. Villarluengo, sheet 543. Memoria del Mapa Geológico de España 1:50.000. Madrid, Servicio de Publicaciones, Ministerio de Industria y Energía, 2ª Serie, 1ª Edición, 45pp.

Giner, J., 1980. Estudio sedimentológico y diagenético de las formaciones carbonatadas del Jurásico de los Catalánides, Maestrazgo y rama aragonesa de la Cordillera Ibérica (sector oriental). PhD Thesis. Barcelona, University of Barcelona, Barcelona, 316pp.

Gómez, J.J., Goy, A., 1998. Unidades litoestratigráficas del tránsito Triásico-Jurásico en la región de Lécera (Zaragoza). Geogaceta, 23, 63-66.

González, A., 1989. Análisis tectosedimentario del terciario del borde SE de la Depresión del Ebro (sector bajoaragonés) y de las cubetas ibéricas marginales. PhD Thesis. Universidad de Zaragoza, Zaragoza, 507pp.

González, A., Guimerà, J., 1993. Sedimentación sintectónica en una cuenca transportada sobre una lámina de cabalgamiento: la cubeta terciaria de Aliaga. Revista de la Sociedad Geológica de España, 6, 151-165.

González, A., Guimerà, J., 1997. Marco estructural de la sedimentación durante el Mioceno inferior en el extremo meridional de la Cuenca del Ebro. In: Calvo, J.P., Morales, J., (eds.). Avances en el conocimiento del Terciario Ibérico. III Congreso del Grupo Español del Terciario. Universidad Complutense de Madrid, Facultad de Ciencias Geológicas y Consejo Superior de Investigaciones Científicas (CSIC), 97-100.

González, A., Guimerà, J., Luzón, A., 1994. Relaciones tectónica-sedimentación en la Zona de Enlace y borde suroriental de la depresión del Ebro. In: González, A. (ed.). Jaca, Guía de Excursiones del II Congreso del Grupo Español del Terciario, 1-134.

González, A., Guimerà, J., Luzón, A., 1998. Edad Oligoceno superior-Mioceno inferior para las superficies de erosión conservadas en el flanco SW de la cubeta de Bordón (Provincia de Teruel, España). Geogaceta, 24, 155-158.

Guimerà, J., 1988. Estudi estructural de l'Enllaç entre la Serralada Ibèrica i la Serralada costanera Catalana. PhD Thesis. Barcelona, University of Barcelona, Barcelona, 600pp.

Guimerà, J., 2004. Cadenas con cobertera: Las Cadenas Ibérica y Costera Catalana. In: Vera, J.A. (ed.). Geología de España. Madrid, Sociedad Geológica de España (SGE) y Instituto Geológico y Minero de España (IGME), 602-607.

Guimerà, J., 2013. Estructura y evolución tectónica de la Cadena Ibérica. In: Simón, J.L., Liesa, C.L. (eds.). XLVII Curso

de Geología Práctica. La Orogenia Alpina en la Cordillera Ibérica. Universidad de Verano de Teruel, 1-9.

Guimerà, J., Álvaro, M., 1990. Structure et évolution de la compression alpine dans la Chaîne Ibérique et la Chaîne Côtière Catalane (Espagne). Bulletin de la Société Géologique de France (8), VI (2), 339-340.

Guimerà, J., Salas, R., 1996. Inversión terciaria de la falla normal mesozoica que limitaba la subcuenca de Galve (Cuenca del Maestrazgo). Geogaceta, 20 (7), 1701-1703.

Guimerà, J., González, A., Salas, R., Sancho, C., 2010. Origin and preservation of the late contractional relief of an intraplate thrust-belt: the NE Iberian Chain (Iberian Peninsula). EGU2010-5137, EGU General Assembly Geophysical Research Abstracts, 12.

Hernández, A., 1985. Teruel, sheet 47. Memoria del Mapa Geológico de España 1:200.000. Madrid, Servicio de Publicaciones, Ministerio de Industria y Energía, 1ª Edición, 192pp.

Lanaja, J.M., 1987. Contribución de la exploración petrolífera al conocimiento de la geología de España. Madrid, Instituto Tecnológico GeoMinero de España, 465pp.

Liesa, C.L., Soria, A.R., Meléndez, N., Meléndez, A., 2006. Extensional fault control on the sedimentation patterns in a continental rift basin: El Castellar Formation, Galve sub-basin, Spain. London, Journal of the Geological Society, 163, 487-498.

López-Gómez, J., Arche, A., Márquez-Aliaga, A., Salas, R., Goy, A., Guimerà, J., Tomás, S., 2005. El Pérmico y el Triásico del Desert de les Palmes, Cordillera Ibérica Oriental, Castellón. Cidaris, 27-28, 5-34.

López-Mir, B., Muñoz, J.A., García-Senz, J., 2015. Extensional salt tectonics in the partially inverted Cotiella post-rift basin (south-central Pyrenees): structure and evolution. International Journal of Earth Sciences, 104 (2), 419-434. DOI: 10.1007/s00531-014-1091-9

Martín, L., Leyva, F., Canérot, J., 1972. Morella, sheet 545. Mapa Geológico de España 1:50.000. Madrid, Servicio de Publicaciones, Ministerio de Industria y Energía, 2ª Serie, 1ª Edición.

Martínez-Abad, J.L., 1991. Cuenca del Maestrazgo. Correlación de sondeos I-I'. In: López, F. (coord.). Estudio geológico del Maestrazgo y de la mitad meridional de los Catalánides. INYPSA y Instituto Geológico y Minero de España (IGME), unpublished.

Navarro-Vázquez, D., Crespo-Zamorano, A., Pérez-Castaño, A., Canérot, J., 1972. Forcall, sheet 544. Mapa Geológico de España 1:50.000. Madrid, Servicio de Publicaciones, Ministerio de Industria y Energía, 2ª Serie, 1ª Edición.

Ortí, F., 1973. El Keuper del Levante Español. Litoestratigrafía, petrología y paleogeografía de la cuenca. PhD Thesis. Barcelona, Universitat de Barcelona, 174pp.

Roca, E., Guimerà, J., 1992. The Neogene structure of the eastern Iberian margin: structural constraints on the crustal evolution of the Valencia through (western Mediterranean). Tectonophysics, 203, 203-218. DOI: 10.1016/0040-1951(92)90224-T

Roca, E., Guimerà, R., Salas, R., 1994. Mesozoic extensional tectonics in the southeast Iberian Chain. Geological Magazine, 131 (2), 155-168.

Salas, R., 1987. El Malm i el Cretaci inferior entre el Massís de Garraf i la Serra d'Espadà. PhD Thesis. Barcelona, Universitat de Barcelona, 345pp.

Salas, R., Casas, A., 1993. Mesozoic extensional tectonics, stratigraphy and crustal evolution during the Alpine cycle of the Eastern Iberian basin. Tectonophysics, 228, 33-35. DOI: 10.1016/0040-1951(93)90213-4

Salas, R., Guimerà, J., 1996. Rasgos estructurales principales de la cuenca cretácica inferior del Maestrazgo (Cordillera Ibérica oriental). Geogaceta, 20 (7), 1704-1706.

Salas, R., Martín-Closas, C., Querol, X., Guimerà, J., Roca, E., 1995. Evolución tectonosedimentaria de las cuencas del Maestrazgo y Aliaga-Penyagolosa durante el Cretácico inferior. In: Salas, R., Martín-Closas, C. (eds.). El Cretácico inferior del Nordeste de Iberia. Barcelona, Universitat de Barcelona, 13-94.

Salas, R., Guimerà, J., Giménez-Montsant, J., Martín-Closas, C., Roca, E., 1997. Mesozoic Rift structure, Stratigraphy and Palaeogene Inversion of the Maestrat basin. Iberian Range (NE Spain). Field trip guide. IGCP Project-369. Comparative evolution of PeriTethyan Rift Basins, Barcelona, Universitat de Barcelona, 70pp.

Salas, R., Guimerà, J., Mas, R., Martín-Closas, C., Meléndez, A., Alonso, A., 2001. Evolution of the Mesozoic Central Iberian Rift System and its Cainozoic inversion (Iberian chain). In: Ziegler, P.A., Cavazza, W., Robertson, A.H.F., Crasquin-Soleau, S. (eds.). Peri-Tethys memoir, 6: Peri-Tethyan Rift/Wrench Basins and Passive Margins. Paris, Mémoires du Muséum National d'Histoire Naturelle, 186, 145-186.

Salas, R., Martín-Closas, C., Delclòs, X., Guimerà, J., Caja, M.A., Mas, R., 2005. Factores principales de control de la sedimentación y los cambios bióticos durante el tránsito Jurásico-Cretácico en la Cadena Ibérica. Geogaceta, 38, 15-18.

Salas, R., García-Senz, J., Guimerà, J., Bover-Arnal, T., 2010. Opening of the Atlantic and development of the Iberian intraplate rift basins during the late Jurassic-early Cretaceous. II Central and North Atlantic Conjugate Margins Conference, 245-248.

San Román, J., Aurell, M., 1992. Paleogeographical significance of the Triasssic-Jurassic unconformity in the north Iberian basin (Sierra del Moncayo, Spain). Palaeogeography, Palaeoclimatology, Palaeoecology, 99 (1-2), 101-117. DOI: 10.1016/0031-0182(92)90009-T

Seillé, H., Salas, R., Pous, J., Guimerà, J., Gallart, J., Torne, M., Romero-Ruiz, I., Diaz, J., Ruiz, M., Carbonell, R., Mas, R., 2015. Crustal structure of an intraplate thrust belt: The Iberian Chain revealed by wide-angle seismic, magnetotelluric soundings and gravity data. Tectonophysics, 663, 339-353. DOI: 10.1016/j.tecto.2015.08.027

Serrano, A., Martínez del Olmo, W., 2004. Estructuras diapíricas de la zona meridional de la Cuenca Vasco-Cantábrica. In: Vera, J.A. (ed.). Geología de España. Madrid, Sociedad

Geológica de España (SGE) y Instituto Geológico y Minero de España (IGME), 334-338.

SIGECO. Sistema de consulta y difusión web de cartografía geológica. Instituto Geológico y Minero de España. Ministerio de Economía y Competitividad, Spain. Available at http://cuarzo.igme.es/sigeco/default.htm (accessed 13 April 2016).

Simón, J.L., 1980. Estructuras de superposición de plegamientos en el borde NE de la cadena Ibérica. Acta Geológica Hispánica, 15 (5), 137-140.

Trell, A., Canérot, J., Martín, M., 1979. Villahermosa del Río, sheet 592. Mapa Geológico de España 1:50.000. Madrid, Servicio de Publicaciones, Ministerio de Industria y Energía, 2ª Serie, 1ª Edición.

Yébenes, A., 1973. Estudio petrogenético de las carniolas de la Cordillera Ibérica. Licentiate Thesis. Madrid, Universidad Complutense de Madrid, 118pp.